Adhirons inhibit immune complex binding to FcγRIIIa with high specificity through competitive and allosteric modes of action.

Authors

James I Robinson[1], Euan W Baxter[1•], Robin L Owen[2•], Maren Thomsen[3•], Darren C Tomlinson[3,4•], Mark P. Waterhouse[1•], Stephanie J Win[1], Joanne E Nettleship[5], Christian Tiede[3], , Richard J Foster[4,6], Raymond J Owens[5], Colin WG Fishwick[4,6], Sarah A. Harris[4,7], Adrian Goldman[3,8], Michael J McPherson[3,4], Ann W Morgan[1]

[1]Leeds Institute of Rheumatic and Musculoskeletal Medicine, School of Medicine, University of Leeds, LS9 7TF and NIHR- Leeds Musculoskeletal Biomedical Research Centre, Leeds Teaching Hospitals NHS Trust

[2]Diamond Light Source, Harwell Science and Innovation Campus, Didcot OX11 0DE

[3]BioScreening Technology Group, School of Molecular and Cellular Biology, University of Leeds, LS2 9JT

[4]Astbury Centre for Structural and Molecular Biology, University of Leeds, LS2 9JT

[5]Oxford Protein Production Facility-UK, Research Complex at Harwell, Rutherford Appleton Laboratory, Oxford OX11 0FA and Division of Structural Biology, Henry Wellcome Building for Genomic Medicine OX3 7BN

[6]School of Chemistry, University of Leeds, LS2 9JT

[7]School of Physics and Astronomy, University of Leeds, LS2 9JT

[8]Faculty of Biological and Environmental Sciences, PO Box 65, University of Helsinki, FIN-0014, Helsinki, Finland

• Contributed equally to this work and should be considered joint second authors.

Correspondence should be addressed to Professor Ann W Morgan, Leeds Institute of Rheumatic and Musculoskeletal Medicine, Wellcome Trust Brenner Building, St James's University Hospital, School of Medicine, University of Leeds, LS9 7TF or Professor Michael McPherson, BioScreening Technology Group, School of Molecular and Cellular Biology, University of Leeds, LS2 9JT

e-mail: a.w.morgan@leeds.ac.uk

m.j.mcpherson@leeds.ac.uk

Telephone 44(0)113 343 8414 / 44(0)113 343 2595

2

ABSTRACT

Protein-protein interactions are essential for the control of cellular functions and critical for regulation of the immune system. One example is the binding of Fc regions of immunoglobulin G (IgG) to the Fc gamma receptors (FcγRs). High sequence identity (98%) between the genes encoding FcγRIIIa (expressed on macrophages and NK cells) and FcγRIIIb (expressed on neutrophils) has prevented development of monospecific agents against these therapeutic targets. We now report the identification of FcγRIIIa-specific artificial binding proteins called Adhirons that block IgG binding and abrogate FcγRIIIa-mediated downstream effector functions in macrophages, namely TNF release and phagocytosis. Cocrystal structures and molecular dynamics simulations have revealed the structural basis of this specificity for two Adhirons, where one binds directly to the Fc binding site, whereas the other acts allosterically. Future studies will use these Adhirons as molecular tools and will evaluate their potential as novel therapeutics.

SIGNIFICANCE STATEMENT

Autoimmune disease pathogenesis is driven by inflammation, induced partly by IgG autoantibody-containing immune complexes binding to Fc gamma receptors (FcγRs). These receptors are widely considered to be valid therapeutic targets in the treatment of autoimmunity. FcγRIIIa is one of a family of highly homologous receptors for IgG antibodies; previous attempts at therapeutic blockade have resulted in off-target effects involving cells which express the almost identical protein FcγRIIIb. Here we report the identification of functionally specific protein-based inhibitors (Adhirons) of FcγRIIIa and the structural/functional basis of their selectivity. As molecular research tools FcγRIIIa-specific Adhirons provide the ability to block IgG interaction with a single receptor. Our findings suggest that highly selective protein-based blocking agents can be readily produced which may have therapeutic applications.

/body

Improved understanding of genetic, genomic and cellular processes underpinning human disease have led to the identification of a multitude of protein-protein interactions that represent potentially important therapeutic targets, frequently for multiple diseases. Drug discovery has traditionally focused on classical enzyme pockets, and chemical libraries are screened to identify inhibitors using biochemical and biophysical assays. Protein-protein interactions are notoriously difficult to target by this approach, since the interfaces frequently comprise large contact surfaces, which generally lack the deep pockets required for traditional medicinal chemistry approaches. In recent years, alternative strategies have emerged including fragment-based approaches to explore the chemical space or the use of peptide-based recognition molecules, such as hydrocarbon-stapled peptides, alpha mimetics, non-antibody protein scaffolds and antibody-aided technologies (reviewed in (1)). Proteomimetic molecules have inherently greater potential to bind to critical interaction interfaces and sterically block protein-protein interactions. Traditional computational-based design tools have tended to focus on orthosteric inhibitors that directly target the interaction site, such as the receptor ligand-binding domain or active site of an enzyme. Novel approaches for therapeutic development include stabilization of protein complexes and identification of allosteric modulators that bind at sites distant to the interacting proteins (2, 3).

Currently, antibodies are the best-studied group of protein-based inhibitors with a wide range of therapeutic humanized monoclonal antibodies already in clinical use (4). However, antibodies are not always ideal as molecular tools due to their multiple domains and chains, poor stability, high production costs and batch-to-batch variation, some of which may be due to glycosylation heterogeneity (5). Artificial binding reagents (protein, RNA and DNA aptamers) are relatively small and make attractive alternatives to antibodies. We have recently established a scaffold consensus protein based on plant cystatins, called Adhiron (9 kDa) which provides a highly stable scaffold (Tm = 101°C) for presenting two variable amino acid sequence regions for molecular recognition (6). These variable regions (VR) form a binding interface analogous to that presented by the complementarity determining regions of an antibody. Adhirons are selected from phage display libraries (>$3x10^{10}$) allowing rapid identification of highly specific reagents that selectively bind to a target and often act as competitive or allosteric inhibitors (7-9). Non-antibody binding proteins tend to recognize binding ‘hot spots’, which are small groups of amino acids on the target protein that contribute the majority of the interaction free energy (10). We propose that Adhirons can be used to study protein function and to disrupt protein-ligand interactions. This unbiased approach may also increase the potential for introducing selectivity where multiple receptors bind to a single ligand, or conversely where multiple ligands bind to a single receptor. We

have explored the potential utility of this approach using human Fcγ Receptors (FcγRs) as a model system.

Human FcγR-ligand interactions constitute a biological system whereby multiple layers of complexity facilitate the fine-tuning of immune responses to infections. Immunoglobulin G (IgG) is the major ligand and mediates both pro- and anti-inflammatory effects following immune complex formation and engagement with different FcγRs. These activating and inhibitory receptors play a central role in the initiation and regulation of many immunological processes, including setting thresholds for B cell activation, recruitment of leukocytes, proinflammatory mediator release, phagocytosis and antibody-dependent cellular cytotoxicity (ADCC) (11, 12). Our genetic studies have demonstrated a number of independent associations with genes in the *FCGR* locus in different autoimmune and inflammatory diseases (13-15). We have also described higher levels of FcγRIIIa on circulating $CD14^{++}$ monocytes in rheumatoid arthritis patients compared with healthy controls, which was correlated with increased TNF release on exposure to immune complexes and inferior treatment outcomes (16). Animal models also provide a strong rationale for targeting FcγRs in autoantibody-mediated inflammatory diseases, including autoantibody/immune complex-induced arthritis (17, 18).

There are six functional human FcγRs subdivided into three classes (FcγRI, FcγRIIa, FcγRIIb, FcγRIIc, FcγRIIIa and FcγRIIIb). Multiple segmental duplications and deletions during hominid evolution have resulted in a family of highly homologous receptors with significant divergence of biological functions from those observed in rodents (19, 20). The level of homology has been a major obstacle for the development of FcγR-specific therapeutics.

A number of FcγR class-specific monoclonal antibodies have been tested in humans, predominantly to block ADCC in immune thrombocytopenia purpura (ITP) (21). An antibody against FcγRIII (CD16-3G8) led to transient increases in platelet count, demonstrating early efficacy. However, in addition to immunogenicity, a number of infusion and atypical hypersensitivity reactions were observed in conjunction with neutrophil and monocyte cytopenias that led to early termination of this program. Although these were believed to be secondary to unwanted engagement of the therapeutic Fc region with FcγRs, these were not abrogated when a humanised anti-FcγR with an aglycosylated Fc was used, suggesting alternative approaches may be required (reviewed in (22)). Blockade of the critical proximal signalling molecule spleen tyrosine kinase (SYK) downstream of several FcγRs initially showed promising efficacy in rheumatoid arthritis (23), chronic lymphocytic leukemia and

non-Hodgkin's lymphoma (24), providing clinical support for therapeutic FcγR blockade in human disease. However, further development in rheumatoid arthritis has been suspended, principally due to adverse off-target events (25).

In this proof of principle study, we have screened two artificial binding protein libraries against a recombinant, glycosylase-treated FcγRIIIa ectodomain and identified several FcγRIIIa-specific Adhirons. We present two Adhirons that cocrystallized with the receptor ectodomain, allowing structures to be solved at atomic resolution by X-ray crystallography and molecular dynamics simulations. One Adhiron bound close to the Fc binding domain (PDB 5ML9), acting as a steric inhibitor, whereas the other recognized an allosteric site and bound in the interdomain hinge region (PDB 5MN2).

Our results demonstrate the feasibility of generating highly-specific inhibitors of protein-ligand interactions which bind novel sites and illustrate the utility of Adhirons in the study of protein function at both a molecular and cellular level.

Results

1. *Identification and characterization of FcγRIIIa-specific Adhirons.*

The extent of the challenge faced when developing specific agents against FcγRIIIa is illustrated by the structural alignment of FcγR crystal structures, demonstrating the high degree of target homology (**Fig. 1a)**. This is particularly true for FcγRIIIa and FcγRIIIb where only two amino acids are consistently different between FcγRIIIa and both common human neutrophil alloantigen types (NA1 and NA2, highlighted in red **Fig. 1b**) of FcγRIIIb, where there are a further four polymorphic amino acids in FcγRIIIb (highlighted in yellow): NA2 has one additional site for N-linked glycosylation than FcγRIIIa (Asn64) and has a difference at residue 18; serine in NA2 and arginine in FcγRIIIa and FcγRIIIb-NA1.

Using recombinant FcγRIIIa protein for phage library screening, a total of 72 randomly chosen Adhirons were tested for binding to FcγRIIIa using phage ELISA after three rounds of selection. Of these 52 gave positive results and DNA sequencing revealed six unique clones. The most frequently recovered Adhirons were expressed as soluble proteins. Detailed analysis of two Adhirons, termed AdF4 and AdG3, is presented in this report. AdG3 differed from AdF4 in terms of primary sequence, being derived from different libraries; AdF4 has an extra variable region on an N-terminal extension (NTE, **Fig. 1c**). We measured the FcγRIIIa-AdF4 and -AdG3 interactions by isothermal titration calorimetry (ITC) which estimated the K_Ds to be 217nM and 2.6μM respectively (**Fig. 1d**). When amine coupled to carboxymethylated dextran sensor chips, the soluble ectodomain of FcγRIIIa interacted with both AdF4 and AdG3 with rapid association and dissociation rates (**Fig. S1a**) and 1:1 stoichiometry, allowing fitting to a Langmuir kinetic model, where calculated K_Ds for AdF4 and AdG3 were 963 nM and 253 nM, respectively. Since kinetic measurements at high analyte concentrations were around the detection limits of the instrument used, we calculated steady state affinity from the same interactions, estimating the K_Ds to be 1.03μM and 2.77μM for AdF4 and AdG3, respectively (**Fig. S1b**). In addition we performed SPR on fully glycosylated and endoglycosidase F1-treated FcγRIIIa immobilised via a biotinylated C-terminal Avitag on streptavidin coated chips. Orientated receptor displayed higher steady state affinity for AdF4 and AdG3 at ~860 and ~680nM respectively, with negligible difference conferred by glycosylation (**Fig S1b**).

2. Adhirons block IgG binding with a high degree of FcγR specificity.

Since primary cells expressing FcγRIIIa also express a number of other FcγRs, human embryonic kidney (HEK)293 cells stably expressing individual FcγRs were constructed to

test the specificity of each Adhiron. Each gene was fused to a C-terminal SNAP tag (26), except FcγRIIIb which is GPI-linked to the membrane. For FcγRIIIa allotypes each C-terminal SNAP domain fusion was co-expressed with the common γ-chain of FcεR to facilitate cell surface expression.

We then assessed blockade of heat-aggregated IgG1 (HAG) binding on stably transfected HEK293 cells. Both AdF4 and AdG3 significantly reduced (p=0.01) HAG binding to FcγRIIIa (158V) (**Fig. 2a** and **b**). Our cellular assays on FcγR specificity demonstrated that AdF4 and AdG3 had only a marginal nonsignificant effect on the binding of HAG to ectopically-expressed FcγRIIa and FcγRIIIb, confirming considerably weaker interactions between the Adhirons and these homologous FcγRs (**Fig. 2a**).

Importantly for therapeutic applications, AdF4 and AdG3 inhibited HAG binding to both the FcγRIIIa-158F and -158V allotypes**.** These Adhirons also displaced bound HAG from FcγRIIIa-158V; the allotype with a greater affinity for IgG1 complexes (**Fig. 2c**)**.**

To understand how the Adhirons blocked FcγRIIIa function and achieved such high specificity, we determined the crystal structures of AdF4 and AdG3 in complex with the FcγRIIIa ectodomain. The crystals belonged to space groups $P2_12_12_1$ (AdF4) and $P2_1$ (AdG3), both diffracting to a resolution of 2.35 Å. Scaling and refinement statistics are provided in **Table 1**. All structures demonstrated that the core Adhiron scaffold maintained its compact structure while the variable regions formed contacts with FcγRIIIa (RMSD less than 0.5 Å in all cases). For clarity of referencing amino acid positions in FcγRs and Adhirons, FcγRIIIa and FcγRIIIb will be referred to as γa- and γb- whereas Adhirons will be referred to as AdG3- and AdF4-, respectively. The two selected Adhirons bound to opposite faces of the FcγRIIIa ectodomain with AdF4 interfacing with the two FcγRIIIa-discriminating residues γa-Gly129 and γa-Tyr140, and AdG3 making contacts with FcγRIIIa extracellular domains 1 and 2.

The FcγRIIIa residues contributing to IgG binding, described in Ferrara *et al.*(27) are depicted in light green on the receptor surface in **Figs. 3a** and **4a**. Analysis of PDB 3SGJ coordinates using PISA (EMBL-EBI), estimated the total buried surface area of this interaction interface to be ~950Å^2 and estimated a solvation free energy gain of -8.4 kcal/mol, with the formation of 10 hydrogen bonds.

3. Adhiron F4-FcγRIIIa cocrystal structure reveals a steric mode of inhibition.

AdF4 residues in the two variable regions, VR1 and VR2, interacted with γa-Ile106-His107

and γa-His119-Asp148. Several residues in the AdF4 NTE (His5 to Ala10) also interfaced with FcγRIIIa. Analysis with PISA (EMBL-EBI) estimated that the total buried surface area of the FcγRIIIa-AdF4 interaction to be ~940Å^2, and estimated a solvation free energy gain of -9.0 kcal/mol, with the formation of 12 direct hydrogen bonds. All hydrogen bond pairings are listed in **Table S1**.

The overlapping buried surface area between IgG Fc and AdF4 totalled about half of the individual interfaces, suggesting that AdF4 probably acts as a competitive inhibitor of IgG (**Fig. S2**).

The AdF4-FcγRIIIa crystal structure shows that the AdF4 binding region includes two amino acids which discriminate between FcγRIIIa and FcγRIIIb - γa-Gly129/γb-Asp129 and γa-Tyr140/γb-His140 **(Fig. 3a)**. To provide atomistic insight into the preference of AdF4 for FcγRIIIa, we used molecular dynamics (MD) simulations to compare the interactions of AdF4 with both FcγRIIIa and FcγRIIIb, by mutating the AdF4-FcγRIIIa complex *in silico* to resemble AdF4-FcγRIIIb-NA2. Simulations were performed in triplicate for 200ns for each complex. Calculations of the RMSD (**Fig. S3**) showed that triplicates remained stable during the timescale of the simulations, and that 200ns was sufficient for the RMSD to converge to a stable value, which indicates that no significant global conformational changes took place.

Simulations were first subjected to atomic fluctuation analysis (**Fig. S4**), a measure of the average per-residue mobility throughout the simulations, which identified that VR2 of AdF4 was more mobile. Visual inspection of simulations around the AdF4 VR2-FcγRIIIa interface confirmed mobility of VR2 and that the aromatic ring of γa-Y132 orientates towards γa-Gly129 in FcγRIIIa simulations and away from γb-Asp129 in FcγRIIIb NA2 simulations (**Fig. 3b** and **c**). This is likely due to steric clash of the tyrosine ring with the γb-Asp129 side chain, causing the ring to move position. In MD simulations, the absence of a sidechain in γa-Gly129 allows the AdF4-Phe57 (VR1) sidechain to sit on top of γa-Gly129. AdF4-Phe57 in this position may also contribute to a hydrophobic pocket centred on AdF4 VR2 and γa-Tyr132. Conversely, the presence of a sidechain in γb-Asp129 leads to steric clash with the AdF4-Phe57 sidechain. AdF4-Phe57 is therefore more mobile in FcγRIIIb-containing simulations (**Fig 3b**), which may further weaken the AdF4 VR2-γa-Tyr132 binding pocket. In summary, AdF4 inhibits IgG binding to FcγRIIIa by steric blocking of the IgG binding site and the specificity mechanism of AdF4 is likely due to the variation at position 129 in FcγRIIIa/b, which leads to steric clash with a number of important binding residues.

4. Adhiron G3-FcγRIIIa cocrystal structures revealed allosteric mode of inhibition

As described above, crystals of FcγRIIIa-AdG3 belonged to space group $P2_1$ with 4 chains in the asymmetric unit (chain A and B: FcγRIIIa; chain C and D: AdG3), chain A and D forming one FcγRIIIa-AdG3 complex and chain B and C the other. Due to having fewer crystallisation contacts than chain A, chain B, and in particular D2 of chain B, is highly flexible resulting in poor local quality of the electron density map and a high average B factor (**Table S2**). The overall RMSD/Cα between the AD and BC complexes is nonetheless only 0.62Å (217 aligned atoms), with the differences entirely distal to the binding interface. Thus, the FcγRIIIa-AdG3 complex formed by chain A and D was used for all following analyses and as the template for MD simulations.

Analysis of the FcγRIIIa-AdG3 cocrystal with PISA (EMBL-EBI) gave a total buried surface area in the interface of ~710 Å^2 (estimated solvation free energy gain of -7.5 kcal/mol). All hydrogen bond pairings are listed in **Table S3**. AdG3 bound to the inter-domain hinge region of FcγRIIIa and there was no overlap with the IgG binding site **(Fig. 4a)**. AdG3 residue Phe52 (VR1) sits in a hydrophobic pocket formed by the main chain of γa-Arg97 and the sidechains of γa-Gln83, Trp98, and in particular forms CH-π interactions with γa-Tyr17 while AdG3 Gly51 [O] forms an H-bond with γa-Val99 [N]. γa-Trp98 intercalates between VR1 and VR2, forming water-mediated interactions to AdG3-Phe52 [O] and to AdG3-Gln83 [O]. The residues in VR2 that form sidechain interactions with FcγRIIIa are Gln83–Asn86. AdG3-Trp84 stacks on top of AdG3-His85, which stacks on top of γa-His87. In addition, they interact with the sidechains of γa-Arg18, γa-Gln83, γa-Glu85, and γa-Thr167. Importantly, γa-Arg18 is a discriminating residue between FcγRIIIa/FcγRIIIb-NA1 and FcγRIIIb-NA2 (γa-Arg18/γb-Ser18) and is key in the binding of AdG3, even though it does *not* interact directly with AdG3. Most of the hydrophilic interactions are *via* bridging water molecules. For instance, Wat1 is coordinated by γa-Tyr17, γa-Glu85 and the [O] of AdG3-His85 such that it is forced into an uncommon, but not disallowed, torsion angle conformation of φ = 59.2° and ψ = -100.1°. This positions the sidechain so that it interacts again *via* a water molecule (Wat37) with the backbone of γa-Val86, and is able to form the π-π-stacking interaction mentioned above. The discriminatory γa-Arg18 is held in place by an ion pair with γa-Glu85, and interacts with Wat1 and Wat3, that in turn interact with the VR2 loop.

Triplicate MD simulations (200ns) of FcγRIIIa and FcγRIIIa mutated *in silico* to resemble FcγRIIIb, in complex with AdG3 were performed. H-bond analysis of the simulations identified a number of intra-molecular H-bonds that form between γa-Arg18 and D2 residues of FcγRIIIa, which facilitate the narrowing of the D1-D2 inter-domain angle. Specifically, γa-Arg18 [O] participates in an intra-molecular H-bond with γa-Gln94 [Nε2], γa-Arg18 [H] with γa-Ala95 [O] and γa-Arg18 [NH1/NH2] with γa-Glu166 [OE1/OE2] **(Table S4)**. In the MD simulations, γa-Arg18 was observed interacting with AdG3-VR2 through an H-bond between the γa-Arg18 [NH1/NH2] atoms and AdG3-Asn86 [OD1]. Conversely, in FcγRIIIb, γa-Ser18 preferred participating in intra-molecular H-bonds with neighbouring residues from D1 of FcγRIIIb (γb-Glu21 and γb-Leu20).

Narrowing of the inter-domain angle likely allows γa-Trp99 to move closer to AdG3, leading to intercalation of γa-Trp99 between VR1 and VR2 and the formation of several inter-molecular H-bonds and an additional intra-molecular H-bond (**Fig 4b, S5**). Conversely, as γb-Ser18 in FcγRIIIb forms only a single weak inter-domain contact, the inter-domain angle does not narrow and γb-Trp99 is unable to form these contacts.

Measurement of the D1-D2 inter-domain angles (described by alpha carbon [Cα] atoms in γa-Gln83, -Trp90 and -Asn169) in unbound FcγRIIIb (1FNL), IgG-FcγRIIIa (3SGJ), and AdG3-FcγRIIIa (5MN2) identified hinge angles of 46°, 53° and 41°, respectively **(Fig. 4c** and **d)**.

To analyse how this change in the angle affects IgG binding, we superimposed the D2 domains (γa-Trp90-Gln174) derived from our x-ray structure 5MN2 on the FcγRIIIa structure bound to IgG (3SGJ). This shows that the overall shape of IgG binding site is not disturbed and that only D2 is involved in binding. However, very subtle small conformational changes upon AdG3 binding prevent IgG binding. For example, the stacking interaction of AdG3-Trp84, AdG3-His85 and γa-His87 stabilises the BC loop (Ile88 – Trp90) in a conformation that prevents AdG3-Trp90 from moving, leading to a steric clash with Pro329 in chain B of IgG. In summary, simulations demonstrated that the presence of γa-Arg18 in FcγRIIIa-AdG3, but not γb-Ser18 in FcγRIIIb-AdG3, allows direct interaction of γa-Arg18 with AdG3 and leads to narrowing of the D1-D2 inter-domain angle through multiple γa-Arg18-mediated inter-domain contacts. This narrowing effectively forms the AdG3 binding interface by bringing VR1, VR2 and γa-Trp99 into close proximity.

Our proposed mechanism of IgG blocking is thus allosteric restraint of the inter-domain angle that typically opens to accommodate IgG-binding (28).

5. Adhirons block downstream effector functions in FcγRIIIa-expressing monocytic cells

We sought to demonstrate that AdF4 and AdG3 could block clinically relevant FcγRIIIa effector functions using the THP-1 monocytic cell line. We characterized the cell line and determined that THP-1 cells were of the *FCGR3A*-158FF, *FCGR2A*-131HH and *FCGR2C*-STP/STP genotype, rendering them incapable of functional FcγRIIc expression. This allowed us to select suitable monoclonal antibodies for evaluation of FcγR expression under different experimental conditions using flow cytometry. Hence staining seen with CD32-3D3 (which recognizes FcγRIIa-131R, FcγRIIb and FcγRIIc but not FcγRIIa-131H) represents FcγRIIb expression in this cell line. Transcriptional analysis also confirmed that FcγRIIb transcript variant 3 (RefSeq NM_001002274) and FcγRIIIa, but not FcγRIIIb, were transcribed thus confirming the anti-CD16 (3G8) staining was a true reflection of FcγRIIIa expression.

Following phorbol myristate acetate (PMA)-differentiation, THP-1 cells demonstrated marked up-regulation of FcγRIIIa (CD16) and increased expression of FcγRIIb (CD32-3D3) along with decreased expression of FcγRIIa (CD32-IV.3) and, to a lesser extent, FcγRI (CD64), compared with resting cells (**Fig. 5a**). The marked increase in FcγRIIIa expression following culture with PMA allowed us to test the ability of the Adhirons to inhibit effector functions in the presence or absence of FcγRIIIa expression.

The contribution of FcγRIIIa to HAG-induced TNF production was determined in both resting and PMA-differentiated THP-1, by assessing the level of inhibition obtained with FcγRIII-specific $F(ab')_2$ fragments (**Fig. 5b**). Our results showed that FcγRIIIa blockade with $F(ab')_2$ fragments resulted in a 34.5% increase in cells showing no TNF production following differentiation with PMA. **Fig. 5b** also shows no demonstrable inhibition in TNF production in resting THP-1 cells that do not express appreciable amounts of FcγRIIIa. We then assessed the ability of AdF4 and AdG3 to inhibit HAG-mediated TNF production. Resting THP-1 and PMA-differentiated THP-1 cells were pre-treated with the Adhirons and assessed for their ability to produce TNF in response to HAG. Each Adhiron demonstrated inhibition of TNF production in PMA-differentiated THP-1 at a level comparable to that observed with the FcγRIIIa-specific $F(ab')_2$ fragment. Resting THP-1 that do not express FcγRIIIa display less than 10% inhibition of HAG-induced TNF production, consistent with the levels seen following blockade with the FcγRIIIa-specific $F(ab')_2$ fragment.

We then compared the ability of Adhirons to inhibit phagocytosis of IgG-opsonized *E. coli* in both resting and PMA-differentiated THP-1 cells and compared this with the level of

inhibition observed following pre-treatment with FcγRIII-specific $F(ab')_2$. Inhibition of phagocytosis by each of the Adhirons was only observed in PMA-differentiated THP-1 where FcγRIIIa was expressed, and at a comparable level to cells treated with FcγRIII $F(ab')_2$, consistent with data on inhibition of TNF production (**Fig. 5c**).

Discussion

We describe the isolation of highly specific steric and allosteric inhibitors of FcγRIIIa using Adhiron technology. These Adhirons specifically block IgG immune complex (HAG) binding to FcγRIIIa, but not the closely-related FcγRIIIb and FcγRIIa, and also inhibit downstream effector functions, such as TNF release and phagocytosis. Whilst there are some FcγR class-specific monoclonal antibodies that recognise epitopes in the IgG binding site, no commercially available antibody is specific for FcγRIIIa. This lack of specificity has been demonstrated *in vivo* when both monocyte and neutrophil cytopenias were observed in clinical trials of the CD16-3G8 monoclonal antibody that recognises both FcγRIIIa (expressed on NK cells and some peripheral blood monocytes) and FcγRIIIb (expressed on neutrophils) (29). Preservation of neutrophil function offers the potential to dampen down inflammatory processes orchestrated by macrophages whilst leaving host immunity to infections afforded by neutrophils intact.

We have identified an Adhiron (AdF4) that binds within the IgG binding site and acts as a highly-specific steric inhibitor of IgG binding to FcγRIIIa, but not to FcγRIIa or FcγRIIIb, as shown by HAG binding assays using HEK293 cells expressing a single FcγR allotype. Elucidation of the structural basis for this specificity may facilitate engineering of CD16 therapeutic antibodies to achieve increased selectivity for FcγRIIIa over FcγRIIIb. Through MD simulations, we have shown that AdF4 specificity for FcγRIIIa is likely focussed around the region containing the FcγRIIIa/b discriminating residue (γa-Gly129/γb-Asp129) highlighting that subtle differences in primary sequence which can lead to local changes in topology which can have knock-on effects on molecular recognition.

A novel allosteric site in the hinge region of FcγRIIIa was recognised by AdG3, which holds the receptor ectodomain in a restricted conformation, preventing the opening of the structure associated with IgG Fc binding and in particular γa-Trp90. A major attraction of targeting allosteric sites is that they may be less evolutionarily conserved, and therefore allosteric inhibitors can potentially be more selective. Interestingly, AdG3, although binding to FcγRIIIa at a seemingly conserved region to FcγRIIIb, showed high cellular specificity to FcγRIIIa. Our proposed mechanism of AdG3 specificity is that the presence of γaArg18 leads to a myriad of intramolecular H-bonds that hold FcγRIIIa in a recognisable conformation which enables the selective interaction of AdG3 with FcγRIIIa rather than FcγRIIIb.

This highlights that even in highly conserved proteins, allosteric regulation could provide a valid method for modulating biological function. Reduced binding of HAG to both FcγRIIIa-158F and 158V allotypes, but not to FcγRIIa or FcγRIIIb, was observed. Pertinently, both Adhirons disrupted complexes of pre-bound HAG to FcγRIIIa 158V as well as blocking HAG binding to receptor pre-treated with Adhiron. As for AdF4, the MD simulations showed that subtle changes in amino acid sequence (γa-Gly129/γb-Asp129 in AdF4 and γa-Arg18/γb-Ser18 in AdG3) leads to multiple, small perturbations in both inter and intra-molecular interactions within the complexes, rather than changing a single definitive interaction at the binding site, such as a salt bridge or a hydrogen bond. The molecular design of Adhirons, which employs a stable scaffold for the constraint of flexible regions of variable amino acid sequence, uses the same successful strategy for generating specific protein-protein interactions as antibodies. The high plasticity of the variable regions, combined with the chemical heterogeneity achievable through the wide variety of sequences generated by phage display, ensures that sufficient biochemical space is explored, as well as sufficient conformational space, to discover Adhirons capable of discriminating between highly homologous receptors. However, the delicate balance of interactions involved implies that rational design of future inhibitors based on structural information alone may not be adequate, and that each Adhiron identified as a binder should be considered unique. Indeed, this may be why loop grafting can result in affinity differences between different scaffolds, for example as observed in (30).

The effect of each Adhiron on clinically relevant FcγRIIIa effector functions was confirmed by the TNF production and phagocytosis assays. Although FcγRI, FcγRIIa and FcγRIIIa are expressed on the monocyte-like THP-1 cells, the inhibition of these downstream functions was correlated with the greatly increased FcγRIIIa expression in THP-1 cells differentiated with PMA. TNF release is a relevant *in vitro* model of receptor signalling since immune complex-activated macrophages have been shown to release large amounts of TNF in rheumatoid arthritis (31).

Adhiron technology therefore, represents a promising methodological approach for the generation of highly stable, easily expressed antibody mimetic reagents with capabilities to modulate protein function and protein-protein interactions. X-ray structures of Adhiron/FcγRIIIa complexes provide a structural basis for understanding the potential mechanism of inhibition. Future studies will be aimed at further dissecting the molecular basis of interaction specificity as well as potential development of therapeutic strategies

including engineering higher affinity, through affinity maturation for example, whilst retaining specificity of Adhirons.

Accession codes.

Coordinates and structure factors have been deposited in the Protein Data Bank under the accession codes 5ML9 and 5MN2.

Scripts and unsolvated trajectories to enable re-creation of the MD simulations are available through a DOI (https://doi.org/10.5518/258).

16

Figure Legends

Figure 1. The challenge of structural homology and the selection of specific protein based inhibitors of FcγRIIIa.

(**a**) Superimposed crystal structures of three FcγR ectodomains are shown as ribbon diagrams in complex with a space filling model of the Fc domain of IgG1. FcγRIIa is shown in yellow (3RY6), FcγRIIIa in purple (3AY4) and FcγRIIIb in green (1T83). (**b**) Structural homology between FcγRIIIa and FcγRIIIb. The four amino acids in yellow differ between the FcγRIIIb NA1 and NA2 allotypes; two amino acids in red discriminate FcγRIIIa from FcγRIIIb and the location of the FcγRIIIa-158F/V allotype is green. The FcγRIIIb-NA2 allotype has an extra N-linked glycosylation site at Asn64. Extracellular domains 1 and 2 are depicted in aqua marine (D1 residues 1-89) and wheat (D2 residues 90-74), respectively. (**c**) The aligned amino acid sequences of AdF4 and AdG3 highlighting the positions of variable region 1 (VR1), variable region 2 (VR2) and the affinity tag (AT). Note that AdF4 has an additional N-terminal extension variable region (NTE). Residue numbering within the variable regions is indicated. (**d**) Isothermal titration calorimetry of the FcγRIIIa-AdF4 and -AdG3 interactions with isotherms and data fits. FcγRIIIa was at 10μM in the sample cell and Adhirons were injected in 2μl additions of 100μM.

Figure 2. Adhirons AdF4 and AdG3 specifically reduce immune complex binding to FcγRIIIa.

Heat-aggregated human IgG (HAG) binding assays utilized HEK293 cells stably expressing the full-length Fcγ receptors. Cells were treated with each Adhiron before the addition of HAG followed by anti-human $F(ab')_2$ fragments labelled with PE; binding was measured by flow cytometry.

(**a**) The top row shows representative examples of the effect of AdF4 and AdG3 on immune complex (HAG) binding on cells expressing FcγRIIa; the unfilled distribution represents the untreated cells and the gray distribution represents binding to cells pre-treated with Adhiron. The filled black region represents background binding of $F(ab')_2$ fragments to the cells. The middle row shows both the Adhirons reduce HAG binding to cells expressing FcγRIIIa alone, whereas the bottom row shows Adhirons had little effect on HAG binding to cells expressing FcγRIIIb.

(**b**) Histograms showing the reproducibility of AdF4 and AdG3 inhibition of HAG binding to FcγRs expressed stably on HEK293 cells. Values are normalized to Adhiron-untreated (HAG only) measurements. Error bars indicate standard deviation within three biological replicates.

(**c**) Representative experiments that demonstrate both Adhirons (AdF4 and AdG3) reduce binding of heat-aggregated IgG1 to both common allotypes of FcγRIIIa -158F and -158V (upper and middle panels). The open black histograms show the binding of HAG to cells expressing FcγRIIIa. The effect of preloading the receptors with Adhirons for one hour before adding HAG is shown as a solid grey histogram. The filled black histograms are controls without HAG. The lower panels show both Adhirons displaced HAG from the 158V allotype when added after HAG.

* P<0.05, *** P<0.001 (two-tailed Student's t-test).

Figure 3. Molecular dynamics simulation reveals molecular basis of interaction specificity of AdF4 for FcγRIIIa over FcγRIIIb. (**a**) Overview of AdF4 (orange) interaction with FcγRIIIa/b (domain 1 in aqua marine, domain 2 in wheat) showing FcγRIIIa/b discriminating residues in red and IgG contacts in light green. N-linked glycans with distinguishable electron density in the crystal structures are depicted as sticks. Zoom box for panel c also shown. (**b**) AdF4 variable region interface in FcγRIIIa and FcγRIIIb from molecular dynamics simulations. AdF4 VR1 and VR2 are depicted as ensembles of snapshots taken at 20ns intervals in representative simulations of the FcγRIIIa- and FcγRIIIb-AdF4 interactions. Interatomic distances between γa/b-Gly/Asp129 [CA] and γa/b-Tyr132 [HH] are illustrated as dashed lines and represented in dynamic measurements in (c). In FcγRIIIa the γa-Tyr132 sidechain orientates towards γa-Gly129, enabling AdF4 VR2 to form stable hydrophobic interactions involving γa-Tyr132 and AdF4-Phe57. In FcγRIIIb the γb-Asp129 sidechain clashes with γb-Tyr132 causing the ring to orientate away from γb-Asp129. γb-Asp129 also clashes with AdF4-Phe57 leading to disruption of the AdF4 VR2 hydrophobic interaction and higher mobility of VR2 and AdF4-Phe57 in FcγRIIIb. **(c)** Interatomic distance d averaged over triplicate MD simulations of FcγRIIIa- and FcγRIIIb-AdF4 interactions.

Figure 4. Molecular basis of AdG3 selectivity for FcγRIIIa. (**a**) Overview of binding position of AdG3 (orange cartoon) to FcγRIII (D1 aqua marine, D2 wheat, IgG contacts in light green, polymorphic residues in yellow, FcγRIIIa discriminatory residues in red). The zoom window for panel **b** is indicated by the black box. (**b**) Molecular dynamics simulation pose of the interaction of AdG3 with FcγRIIIa (purple sticks) and FcγRIIIb (green sticks). γa-Trp98 intercalates between AdG3 VR1 and VR2 resulting in several stable intermolecular H-bonds, whereas in FcγRIIIb these contacts did not form in the MD simulations. (**c**) Cartoon representation of FcγRIIIa (aqua marine and wheat) interacting with IgG Fc (salmon). The interdomain angle Θ is described by lines connecting the [CA] of γa-Trp90 at the top of the

hinge, and the [CA] of Asn169 in D2 and the [CA] of Gln83 in D1. Mode vectors describing the allosteric change from the IgG-bound state to the AdG3-bound state are represented as blue arrows. Mode vectors shorter than 3Å not shown. (**d**) Schematic representation of the allosteric change induced by AdG3. Unbound FcγRIII (PDB 1FNL) describes a D1-D2 interdomain angle θ of 46° which opens to 53° on interaction with IgG Fc. FcγRIIIa interaction with AdG3 narrows the D1-D2 angle by 12° to 41° and we hypothesize that this allosteric shift causes sufficient deformation of the IgG Fc binding site to induce IgG Fc displacement.

Figure 5. Adhirons are effective inhibitors of FcγRIIIa – dependent functions. (**a**) FACs profiles for resting, monocytic THP-1 cells (left side) and PMA-differentiated, macrophage-like THP-1 cells (right side). In each case, the specific antibody staining is shown as an unfilled distribution whereas the isotype control staining is shown as a filled distribution. The high affinity FcγRIa (CD64) is reduced in differentiated THP-1 cells, along with the activatory FcγRIIa (CD32-IV.3). The inhibitory FcγRIIb is upregulated in differentiated cells along with FcγRIIIa. **(b)** Adhirons were more effective in blocking HAG-induced TNF release in differentiated cells (upper right panel) than undifferentiated (upper left panel), confirming their specificity for FcγRIIIa. This is represented as an increase in the percentage of TNF negative cells. The upper panels also show blocking $F(ab')_2$ fragments against FcγRIIIa inhibit TNF production only in differentiated THP-1 cells. $F(ab')_2$ fragments against FcγRIII (CD16) are far more effective in differentiated cells (upper panel, right) reflecting the differences in FcγRIIIa expression, shown in **a**. $F(ab')_2$ fragments from preimmune serum had no effect on TNF production. The lower panels show both Adhirons are as effective in reducing phagocytosis of IgG opsonised *E Coli* as $F(ab')_2$ fragments in differentiated THP-1 cells.

Acknowledgements

We acknowledge the University of Leeds and Leeds Teaching Hospitals NHS Trust funding for the Leeds Biomedical Health Research Centre BioScreening Technology Group (BSTG). We are grateful to Mr. Thomas Taylor of the BSTG for excellent technical support. ITC was performed in the Astbury Biomolecular Interactions Facility, supported by the Wellcome Trust, 094232/Z/10/Z. The work undertaken on beamline I24 at Diamond Light Source was under proposal NT5969. The Medical Research Council (grant MR/K018779/1) supported the Oxford Protein Production Facility. The research was also supported by Arthritis Research UK (19764), the National Institute for Health Research (NIHR) Leeds Biomedical Research Centre and the Ann Wilks Memorial fund. The views expressed are those of the

author(s) and not necessarily those of the NHS, the NIHR or the Department of Health. This work was further supported by a grant by Marie Skłodowska-Curie Actions in Horizon 2020 (to MT).

Contributions

A.W.M., M.J.McP. and J.I.R. conceived the project, analyzed the data and wrote the paper, with input from all the other authors. Protein structure determination was performed by R.L.O with additional refinement carried out by M.T., A.G. and further analyses performed by J.I.R., M.T., A.G., R.F. and C.W.G.F. Molecular dynamics simulations were performed by M.P.W and S.A.H. Cloning was performed by J.I.R., J.E.N. and E.W.B. and protein expression and crystallization were performed by J.E.N. and R.J.O. Adhiron screening was performed by C.T. and D.C.T. Cellular assays were performed by S.J.W. and E.W.B. J.I.R. performed the biophysical kinetic characterization of the receptor-Adhiron interactions. J.I.R., D.C.T., E.B., A.W.M. and M.J.McP. made considerable contributions to other experiments, writing and editing the paper, and A.G. to writing the paper.

Competing Financial Interests

The University of Leeds has licensed Adhirons (also referred to as Affimer Type II) to Avacta Life Sciences Ltd.

References

1. Milroy, L.-G., Grossmann, T.N., Hennig, S., Brunsveld, L. & Ottmann, C. Modulators of Protein–Protein Interactions. Chemical Reviews 114, 4695-4748 (2014).

2. Higueruelo, A.P., Jubb, H. & Blundell, T.L. Protein–protein interactions as druggable targets: recent technological advances. Current Opinion in Pharmacology 13, 791-796 (2013).

3. Jubb, H., Higueruelo, A.P., Winter, A. & Blundell, T.L. Structural biology and drug discovery for protein–protein interactions. Trends in Pharmacological Sciences 33, 241-248 (2012).

4. Reichert, J.M., Rosensweig, C.J., Faden, L.B. & Dewitz, M.C. Monoclonal antibody successes in the clinic. Nat Biotechnol 23, 1073-1078 (2005).

5. Vlasak, J. & Ionescu, R. Heterogeneity of Monoclonal Antibodies Revealed by Charge-Sensitive Methods. Current Pharmaceutical Biotechnology 9, 468-481 (2008).

6. Tiede, C. et al. Adhiron: a stable and versatile peptide display scaffold for molecular recognition patterns. Protein Engineering Design and Selection 27, 145-155 (2014).

7. Sharma, R. et al. Label-free electrochemical impedance biosensor to detect human interleukin-8 in serum with sub-pg/ml sensitivity. Biosensors and Bioelectronics 80, 607-613 (2016).

8. Rawlings, A.E. et al. Phage display selected magnetite interacting Adhirons for shape controlled nanoparticle synthesis. Chemical Science 6, 5586-5594 (2015).

9. Kyle, H.F. et al. Exploration of the HIF-1[small alpha]/p300 interface using peptide and Adhiron phage display technologies. Molecular BioSystems 11, 2738-2749 (2015).

10. Modell, A.E., Blosser, S.L. & Arora, P.S. Systematic Targeting of Protein-Protein Interactions. Trends in Pharmacological Sciences 37, 702-713.

11. Nimmerjahn, F. & Ravetch, J.V. Fcg receptors as regulators of immune responses. Nat Rev Immunol 8, 34-47 (2008).

12. Hogarth, P.M. & Pietersz, G.A. Fc receptor-targeted therapies for the treatment of inflammation, cancer and beyond. Nat Rev Drug Discov 11, 311-331 (2012).

13. Morgan, A.W. et al. Association of FCGR2A and FCGR2A-FCGR3A haplotypes with susceptibility to giant cell arteritis. Arthritis Research & Therapy 8, R109 (2006).

14. Robinson, J.I. et al. Association of FCGR3B, but not FCGR3A copy number, with susceptibility to rheumatoid arthritis: functional correlation with reduced neutrophil Fc gamma RIIIb expression. Immunology 131, 123 (2010).

15. Willcocks, L.C. et al. Copy number of FCGR3B, which is associated with systemic lupus erythematosus, correlates with protein expression and immune complex uptake. Journal of Experimental Medicine 205, 1573-1582 (2008).

16. Cooper, D.L. et al. FcgRIIIa expression on monocytes in rheumatoid arthritis: role in immune-complex stimulated TNF production and non-response to methotrexate therapy. PLoS ONE 7, e28918 (2012).

17. Ji, H. et al. Arthritis critically dependent on innate immune system players. Immunity 16, 157-168 (2002).

18. Kleinau, S., Martinsson, P. & Heyman, B. Induction and suppression of collagen-induced arthritis is dependent on distinct Fcg receptors. J Exp Med 191, 1611-1616 (2000).

19. Qiu, W.Q., de Bruin, D., Brownstein, B.H., Pearse, R. & Ravetch, J.V. Organisation of the human and mouse low-affinity FcgR genes: duplication and recombination. Science 248, 732-735 (1990).

20. Machado, L.R. et al. Evolutionary history of copy-number-variable locus for the low-affinity Fc receptor: mutation rate, autoimmune disease, and the legacy of helminth infection. American Journal of Human Genetics 90, 973-985 (2012).

21. Clarkson, S.B. et al. Treatment of refractory immune thrombocytopenic purpura with an anti-Fc gamma-receptor antibody. New England Journal of Medicine 314, 1236-1239 (1986).

22. Bosques, C.J. & Manning, A.M. Fc-gamma receptors: attractive targets for autoimmune drug discovery searching for intelligent therapeutic designs. Autoimmunity Reviews 15, 1081-1088 (2016).

23. Weinblatt, M.E. et al. Effects of Fostamatinib (R788), an Oral Spleen Tyrosine Kinase Inhibitor, on Health-related Quality of Life in Patients with Active Rheumatoid Arthritis: Analyses of Patient-reported Outcomes from a Randomized, Double-blind, Placebo-controlled Trial. Journal Of Rheumatology 40, 369-378 (2013).

24. Friedburg, J.W. et al. Inhibition of Syk with fostamatinib disodium has significant clinical activity in non-Hodgkin lymphoma and chronic lymphocytic leukemia. Blood 115, 2578-2585 (2010).

25. MacFarlane, L.A. & Todd, D.J. Kinase inhibitors: The next generation of therapies in the treatment of rheumatoid arthritis. International Journal of Rheumatic Diseases 17, 359-368 (2014).

26. Keppler, A. et al. A general method for the covalent labeling of fusion proteins with small molecules in vivo. Nat Biotech 21, 86-89 (2003).

27. Ferrara, C. et al. Unique carbohydrate-carbohydrate interactions are required for high affinity binding between FcgRIII and antibodies lacking core fucose. Proceedings of the National Academy of Sciences 108, 12669-12674 (2011).

28. Woof, J.M. & Burton, D.R. Human antibody-Fc receptor interactions illuminated by crystal structures. Nat Rev Immunol 4, 89-99 (2004).

29. Nakar, C.T. & Bussel, J.B. 3G8 and GMA161, Anti FcγRIII Inhibitory Monoclonal Antibodies in the Treatment of Chronic Refractory ITP. (Summary of 2 Pilot Studies). Blood 114, 2404-2404 (2009).

30. Vita, C. et al. Novel miniproteins engineered by the transfer of active sites to small natural scaffolds. Biopolymers 47, 93-100 (1998).

31. Cassatella, M.A. et al. Soluble TNF-like cytokine (TL1A) production by immune complexes stimulated monocytes in rheumatoid arthritis.[Erratum appears in J Immunol. 2007 Jul 15;179(2):1390 Note: da Silva, Gabriela Pereira [corrected to Pereira-da-Silva, Gabriela]]. Journal of Immunology 178, 7325-7333 (2007).

32. Berrow, N.S., Alderton, D. & Owens, R.J. The Precise Engineering of Expression Vectors Using High-Throughput In-Fusiontrade mark PCR Cloning. Methods Mol Biol 498, 75-90 (2009).

33. Bird, L.E. High throughput construction and small scale expression screening of multi-tag vectors in Escherichia coli. Methods 55, 29-37 (2011).

34. Nettleship, J.E., Rahman-Huq, N. & Owens, R.J. The production of glycoproteins by transient expression in mammalian cells. Methods Mol Biol 498, 245-263 (2009).

35. Chomczynski, P. & Sacchi, N. Single-step method of RNA isolation by acid guanidinium thiocyanate -phenol-chloroform extraction. Analytical Biochemistry 162, 156-159 (1987).

36. Warmerdam, P.A.M. et al. Interaction of a human FcgRIIb1 (CD32) isoform with murine and human IgG subclasses. Int Immunol 5, 239-247 (1993).

37. Daeron, M. et al. The same tyrosine-based inhibition motif, in the intracytoplasmic domain of Fc gamma RIIB, regulates negatively BCR-, TCR-, and FcR-dependent cell activation. Immunity 3, 635-646 (1995).

38. Morgan, A.W. et al. Analysis of Fcγ Receptor haplotypes in rheumatoid arthritis. FCGR3A remains a major susceptibility gene at this locus with an additional contribution from FCGR3B. Arthritis Research & Therapy 8, R5 (2006).

39. Metes, D. et al. Expression of functional CD32 molecules on human NK cells is determined by an allelic polymorphism of the FcgRIIC gene. Blood 91, 2369-2380 (1998).

40. Walter, T.S. et al. A procedure for setting up high-throughput nanolitre crystallization experiments. Crystallization workflow for initial screening, automated storage, imaging and optimization. Acta Crystallogr D Biol Crystallogr. 61, 651-657 (2005).

41. Kabsch, W. XDS. Acta Crystallographica Section D 66, 125-132 (2010).

42. Evans, P.R. & Murshudov, G.N. How good are my data and what is the resolution? Acta Crystallographica Section D 69, 1204-1214 (2013).

43. McCoy, A.J. et al. Phaser crystallographic software. Journal of Applied Crystallography 40, 658-674 (2007).

44. Afonine, P.V. et al. Towards automated crystallographic structure refinement with phenix.refine. Acta Crystallographica Section D 68, 352-367 (2012).

45. Emsley, P., Lohkamp, B., Scott, W.G. & Cowtan, K. Features and development of Coot. Acta Crystallographica Section D 66, 486-501 (2010).

46. Tina, K.G., Bhadra, R. & Srinivasan, N. PIC: Protein Interactions Calculator. Nucleic Acids Res 35, W473-W476 (2007).

47. Case, D.A. et al. AMBER 14, University of California, San Francisco. (2014).

48. Maier, J.A. et al. ff14SB: Improving the Accuracy of Protein Side Chain and Backbone Parameters from ff99SB. Journal of Chemical Theory and Computation 11, 3696-3713 (2015).

49. Kirschner, K. N. et al. GLYCAM06: A generalizable biomolecular force field. Carbohydrates. J. Comput. Chem., 29, 622–655. 2008,

50. Prokop, M., Adam, J., Kříž, Z., Wimmerová, M. & Koča, J. TRITON: a graphical tool for ligand-binding protein engineering. Bioinformatics 24, 1955-1956 (2008).

51. Humphrey, W., Dalke, A. & Schulten, K. VMD: visual molecular dynamics. J Mol Graph 14, 33-8, 27-8 (1996).

52. The PyMOL Molecular Graphics System, Version 1.2r3pre. (Schrödinger, LLC).

Fig. 1.

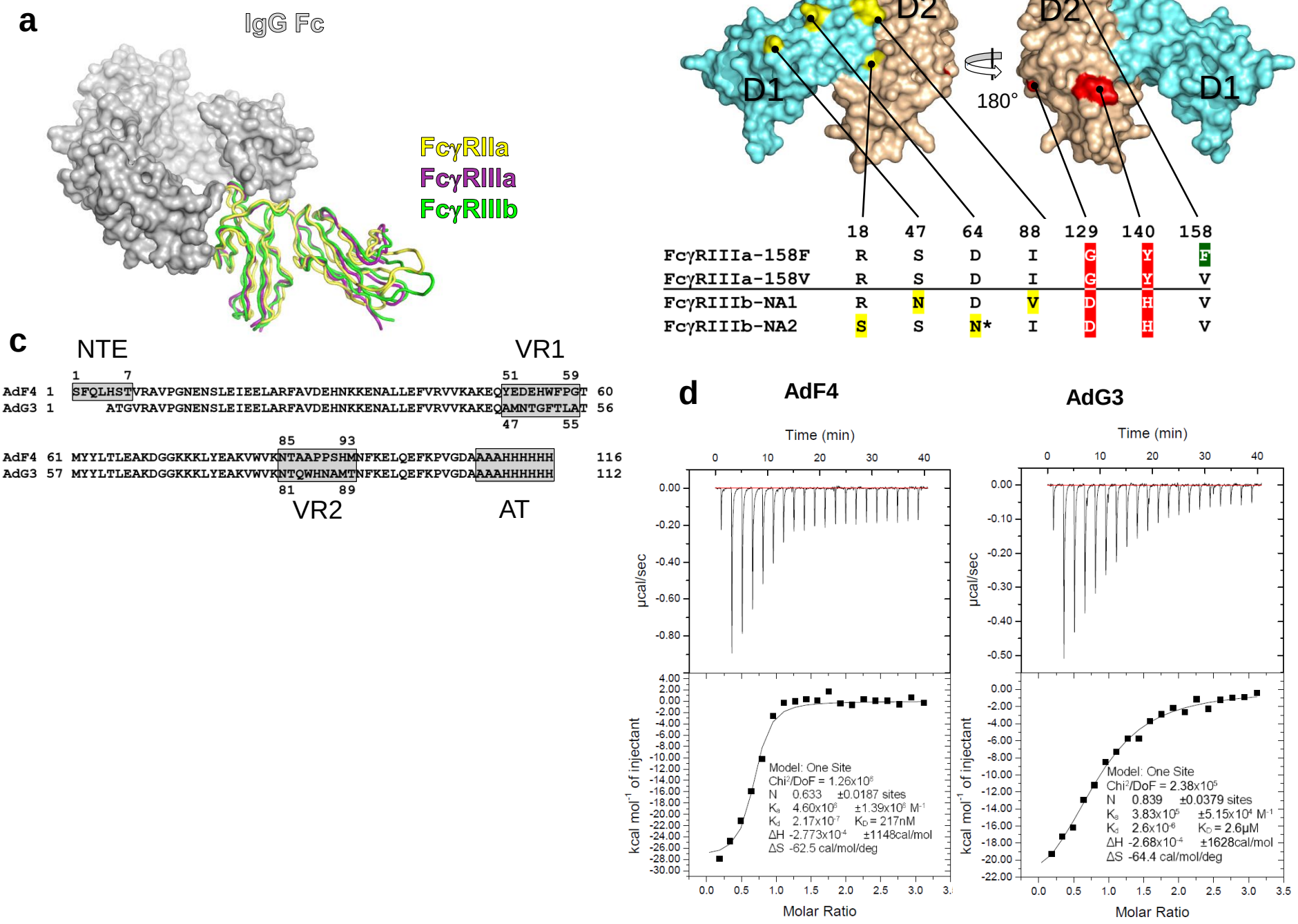
a
IgG Fc
FcγRIIa
FcγRIIIa
FcγRIIIb
b
D2
D1
180°
18 47 64 88 129 140 158
FcγRIIIa-158F R S D I G Y F
FcγRIIIa-158V R S D I G Y V
FcγRIIIb-NA1 R N D V D H V
FcγRIIIb-NA2 S S N* I D H V
c
NTE
VR1
VR2
AT
AdF4 1 SFQLHSTVRAVPGNENSLEIEELARFAVDEHNKKENALLEFVRVVKAKEQYEDEHWFPGT 60
AdG3 1 ATGVRAVPGNENSLEIEELARFAVDEHNKKENALLEFVRVVKAKEQAMNTGFTLAT 56
AdF4 61 MYYLTLEAKDGGKKKLYEAKVWVKNTAAPPSHMNFKELQEFKPVGDAAAAHHHHH 116
AdG3 57 MYYLTLEAKDGGKKKLYEAKVWVKNTQWHNAMTNFKELQEFKPVGDAAAAHHHHH 112
d
AdF4
AdG3
Time (min)
µcal/sec
kcal mol-1 of injectant
Molar Ratio
Model: One Site
Chi²/DoF = 1.26x10⁶
N 0.633 ±0.0187 sites
Kd 4.60x10⁶ ±1.39x10⁶ M⁻¹
Kd 2.17x10⁻⁷ KD = 217nM
ΔH -2.773x10⁻⁴ ±1148cal/mol
ΔS -62.5 cal/mol/deg
Chi²/DoF = 2.38x10⁵
N 0.839 ±0.0379 sites
Kd 3.83x10⁵ ±5.15x10⁴ M⁻¹
Kd 2.6x10⁻⁶ KD = 2.6µM
ΔH -2.68x10⁻⁴ ±1628cal/mol
ΔS -64.4 cal/mol/deg

Fig. 2.

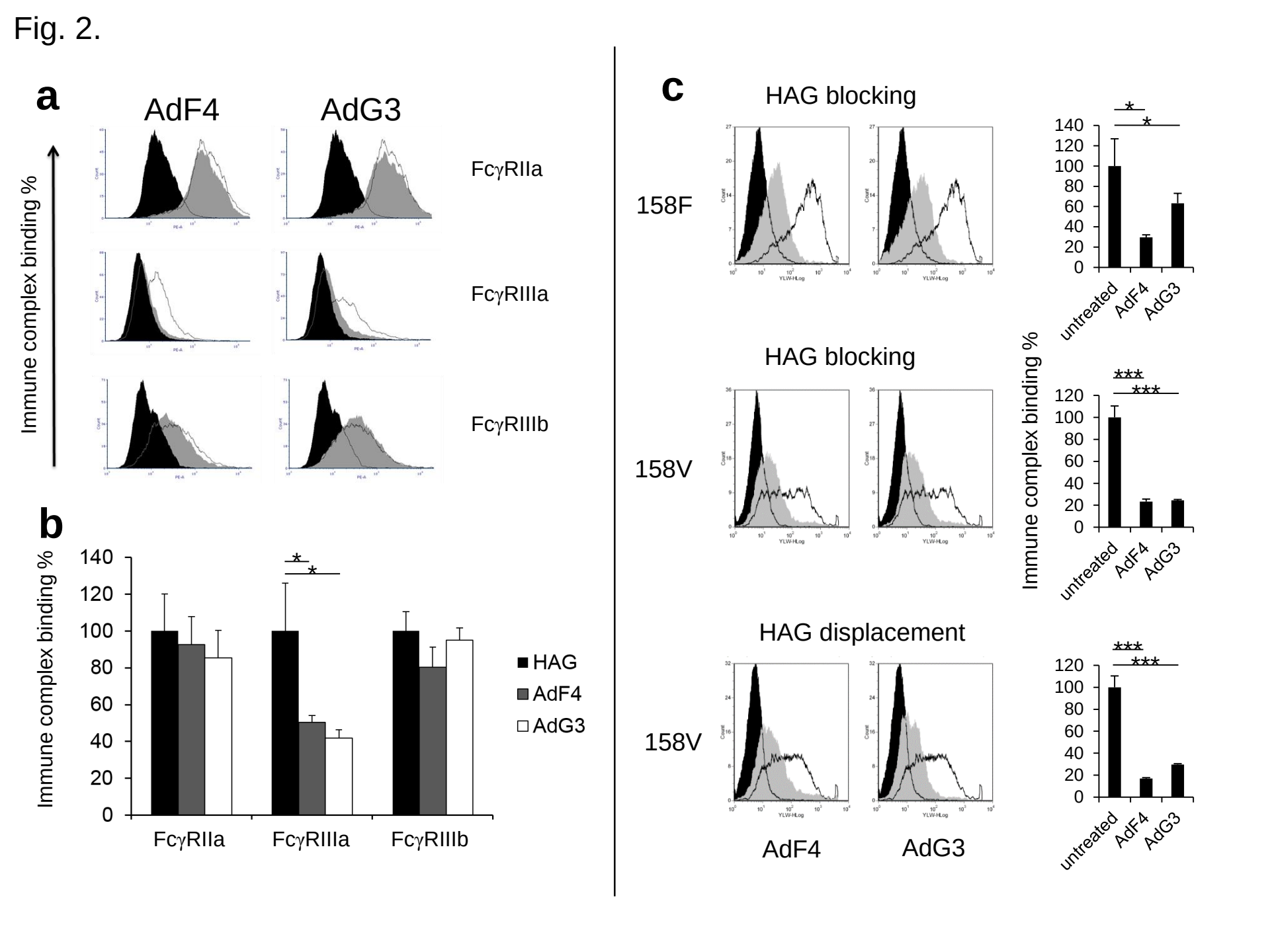
a
AdF4
AdG3
FcγRIIa
FcγRIIIa
FcγRIIIb
Immune complex binding %
b
Immune complex binding %
140
120
100
80
60
40
20
0
*
*
FcγRIIa
FcγRIIIa
FcγRIIIb
HAG
AdF4
AdG3
c
HAG blocking
158F
HAG blocking
158V
HAG displacement
158V
AdF4
AdG3
Immune complex binding %
untreated
AdF4
AdG3
***

Fig. 3.

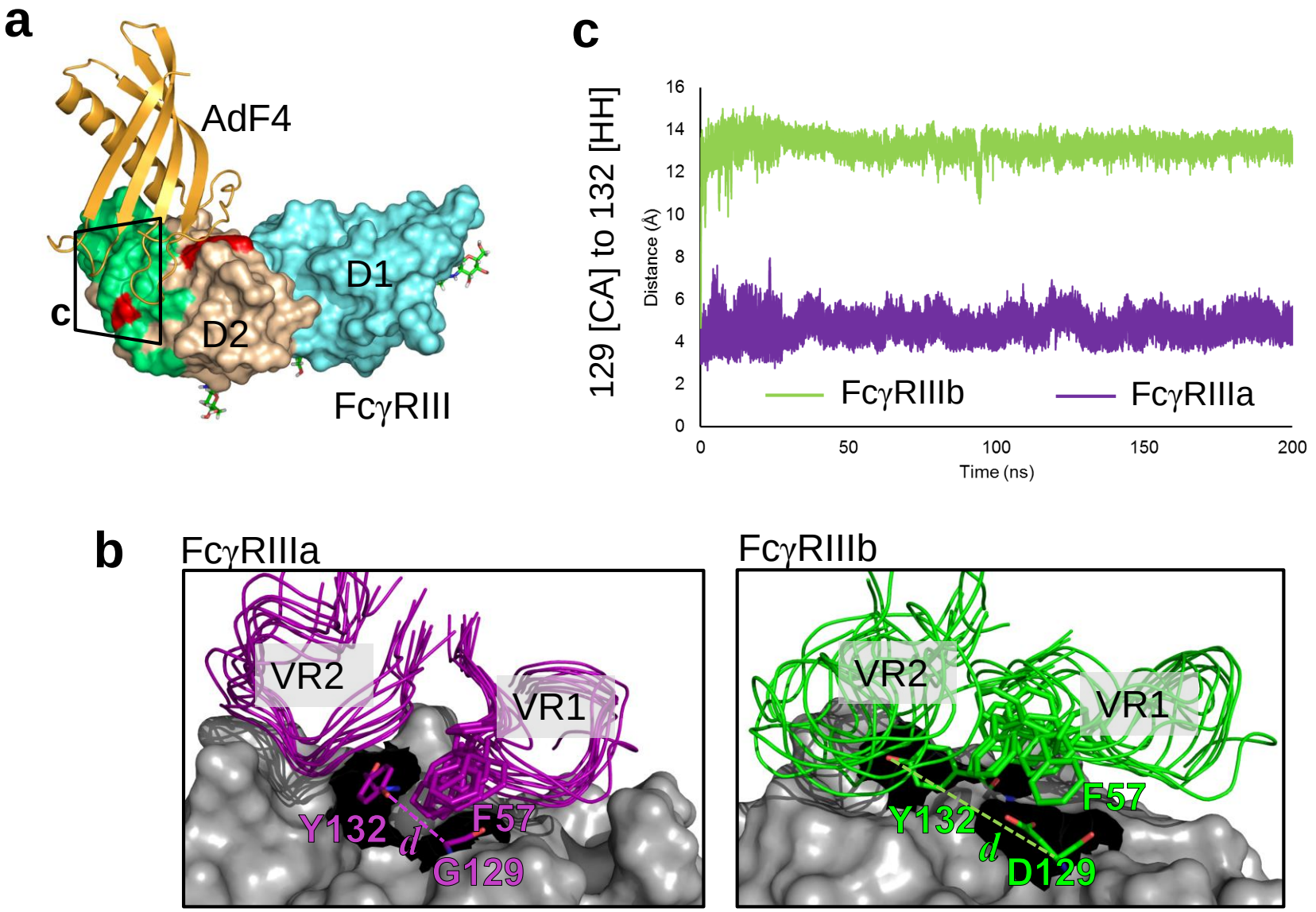
a
AdF4
D1
D2
c
FcγRIII
c
129 [CA] to 132 [HH]
Distance (Å)
16
14
12
10
8
6
4
2
0
0
50
100
150
200
Time (ns)
FcγRIIIb
FcγRIIIa
b
FcγRIIIa
VR2
VR1
Y132
d
F57
G129
FcγRIIIb
VR2
VR1
F57
Y132
d
D129

Fig. 4.

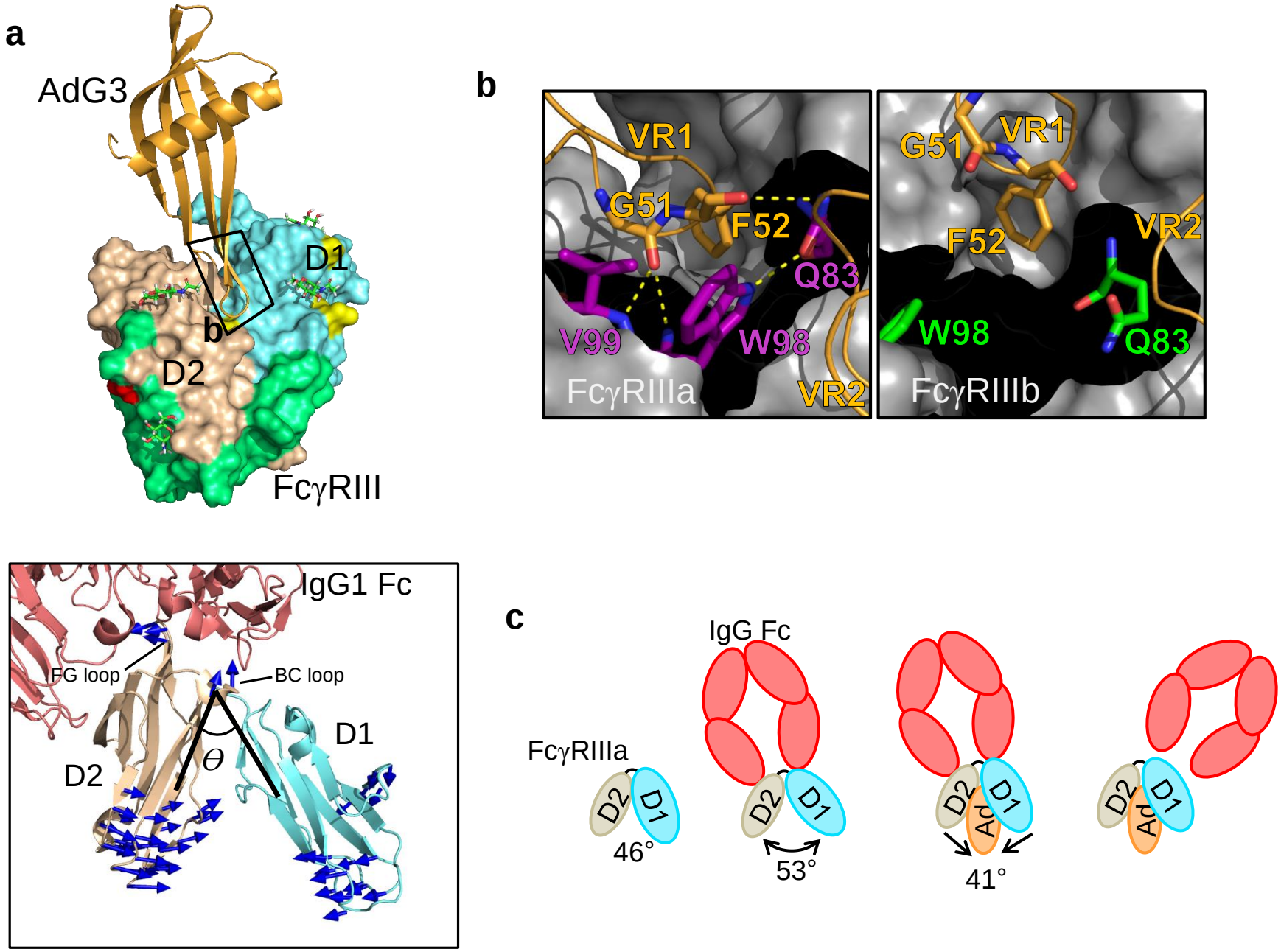
a
AdG3
D1
b
D2
FcγRIII
b
VR1
G51
F52
Q83
V99
W98
FcγRIIIa
VR2
G51
VR1
F52
VR2
W98
Q83
FcγRIIIb
c
IgG1 Fc
FG loop
BC loop
D1
D2
θ
c
IgG Fc
FcγRIIIa
D2
D1
46°
D2
D1
53°
D2
Ad
D1
41°
D2
Ad
D1

Fig. 5.

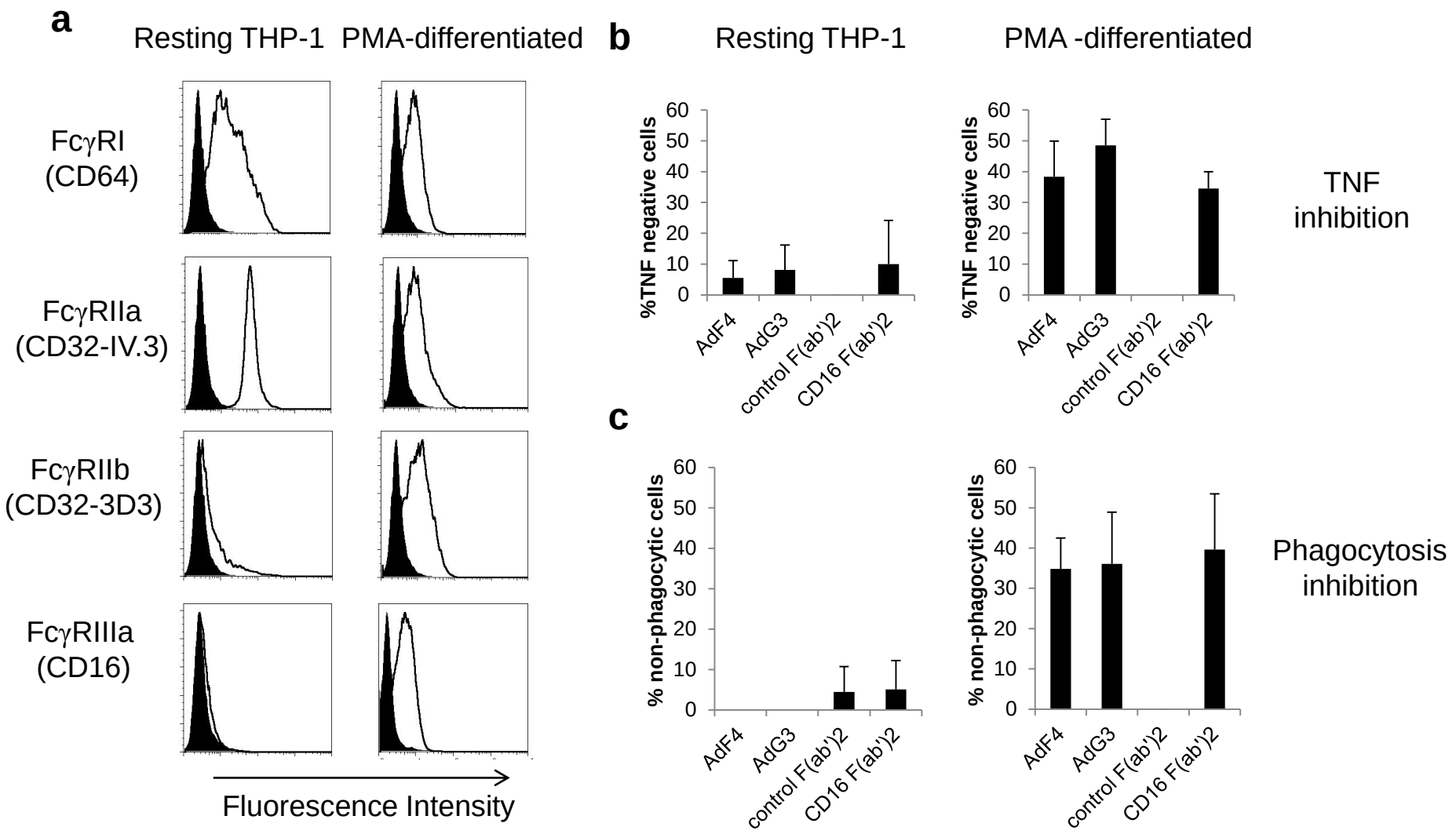
a
Resting THP-1
PMA-differentiated
FcγRI (CD64)
FcγRIIa (CD32-IV.3)
FcγRIIb (CD32-3D3)
FcγRIIIa (CD16)
Fluorescence Intensity
b
Resting THP-1
PMA -differentiated
%TNF negative cells
0
10
20
30
40
50
60
AdF4
AdG3
control F(ab')2
CD16 F(ab')2
TNF inhibition
c
% non-phagocytic cells
Phagocytosis inhibition

Fig. S1.

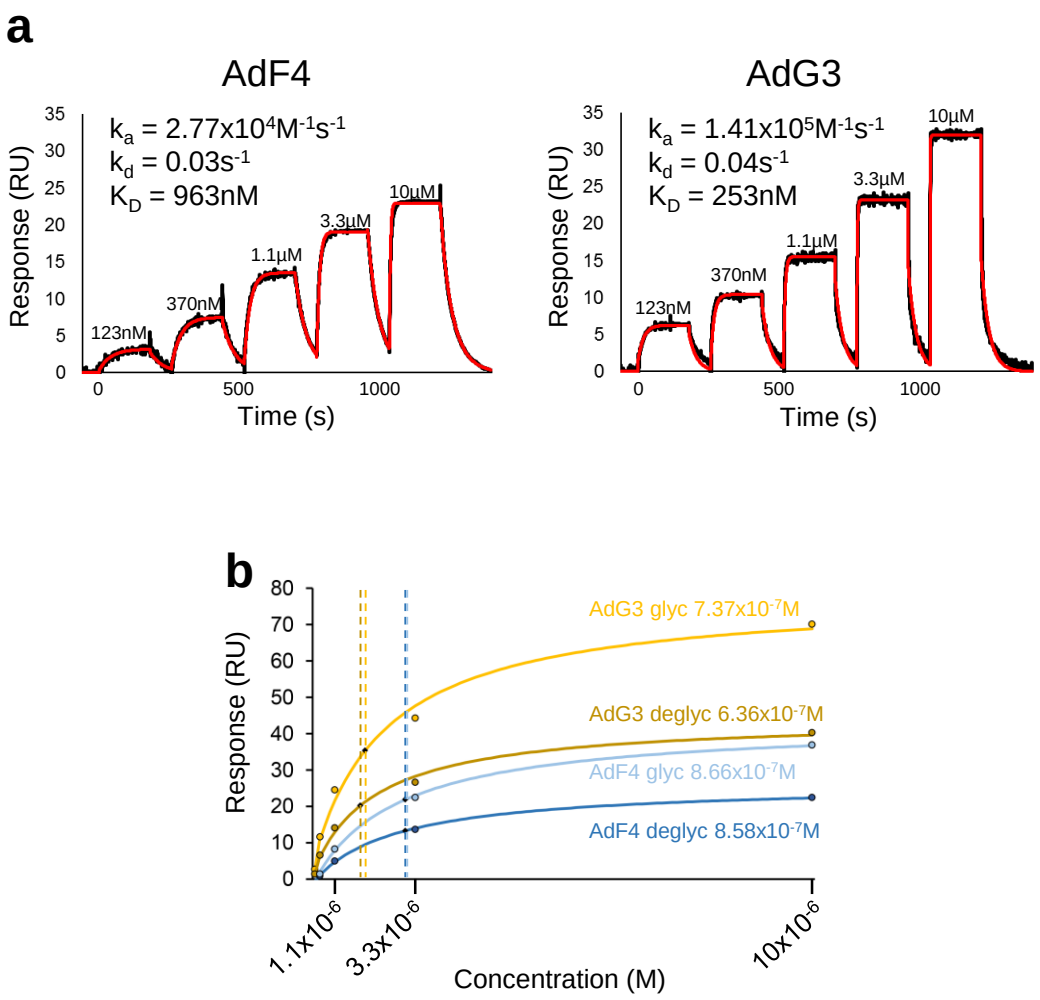
a
AdF4
k_a = 2.77x10^{4}M^{-1}s^{-1}
k_d = 0.03s^{-1}
K_D = 963nM
123nM
370nM
1.1µM
3.3µM
10µM
Response (RU)
Time (s)
AdG3
k_a = 1.41x10^{5}M^{-1}s^{-1}
k_d = 0.04s^{-1}
K_D = 253nM
123nM
370nM
1.1µM
3.3µM
10µM
Response (RU)
Time (s)
b
AdG3 glyc 7.37x10^{-7}M
AdG3 deglyc 6.36x10^{-7}M
AdF4 glyc 8.66x10^{-7}M
AdF4 deglyc 8.58x10^{-7}M
Response (RU)
1.1x10^{-6}
3.3x10^{-6}
10x10^{-6}
Concentration (M)

Fig. S2.

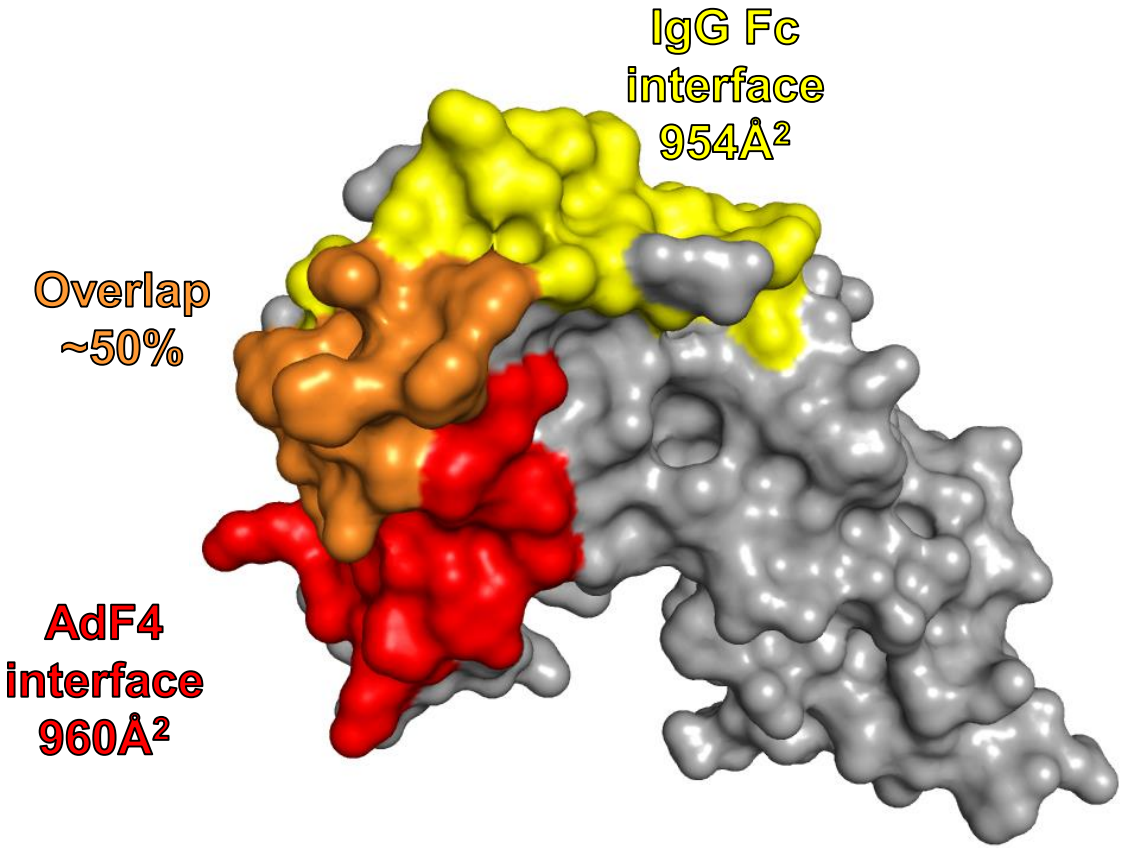

Fig. S3.

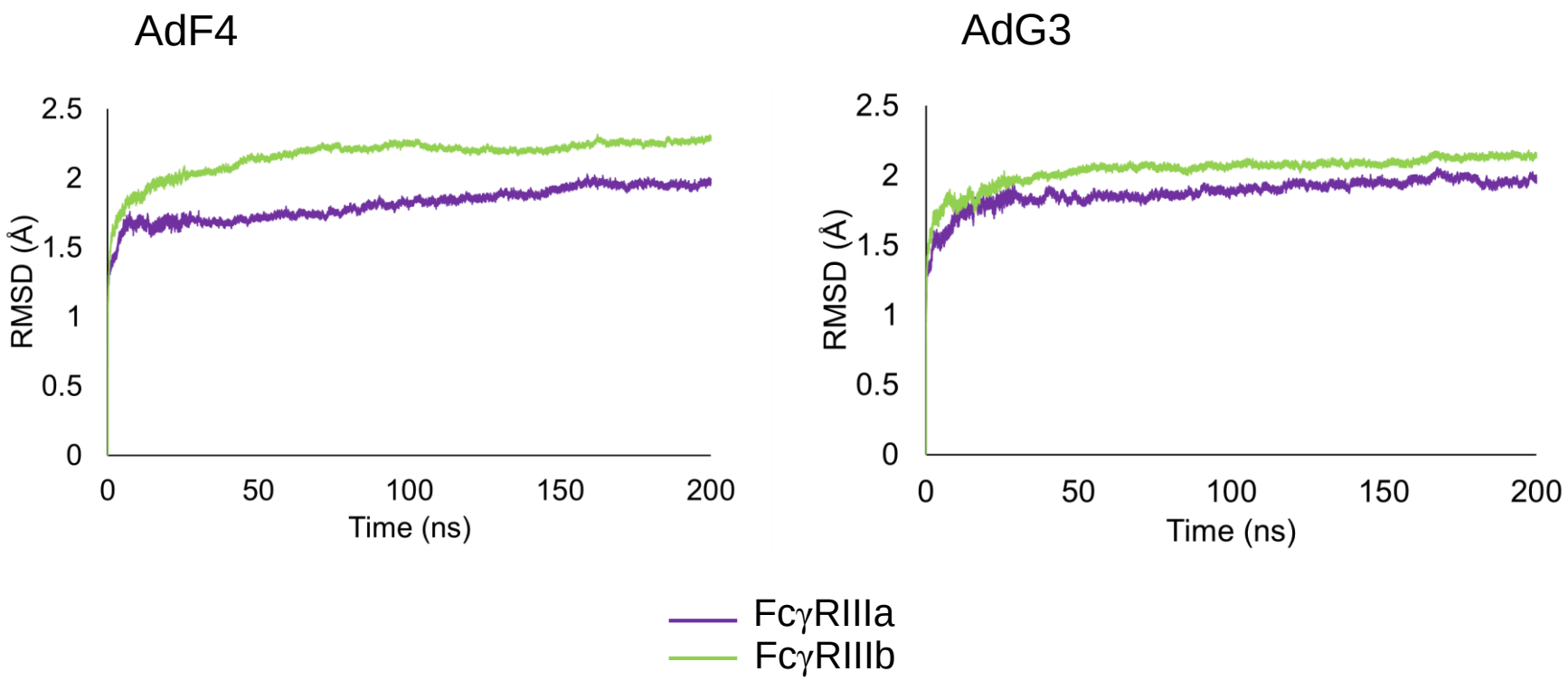
AdF4
AdG3
RMSD (Å)
Time (ns)
0
0.5
1
1.5
2
2.5
0
50
100
150
200
FcγRIIIa
FcγRIIIb

Fig. S4.

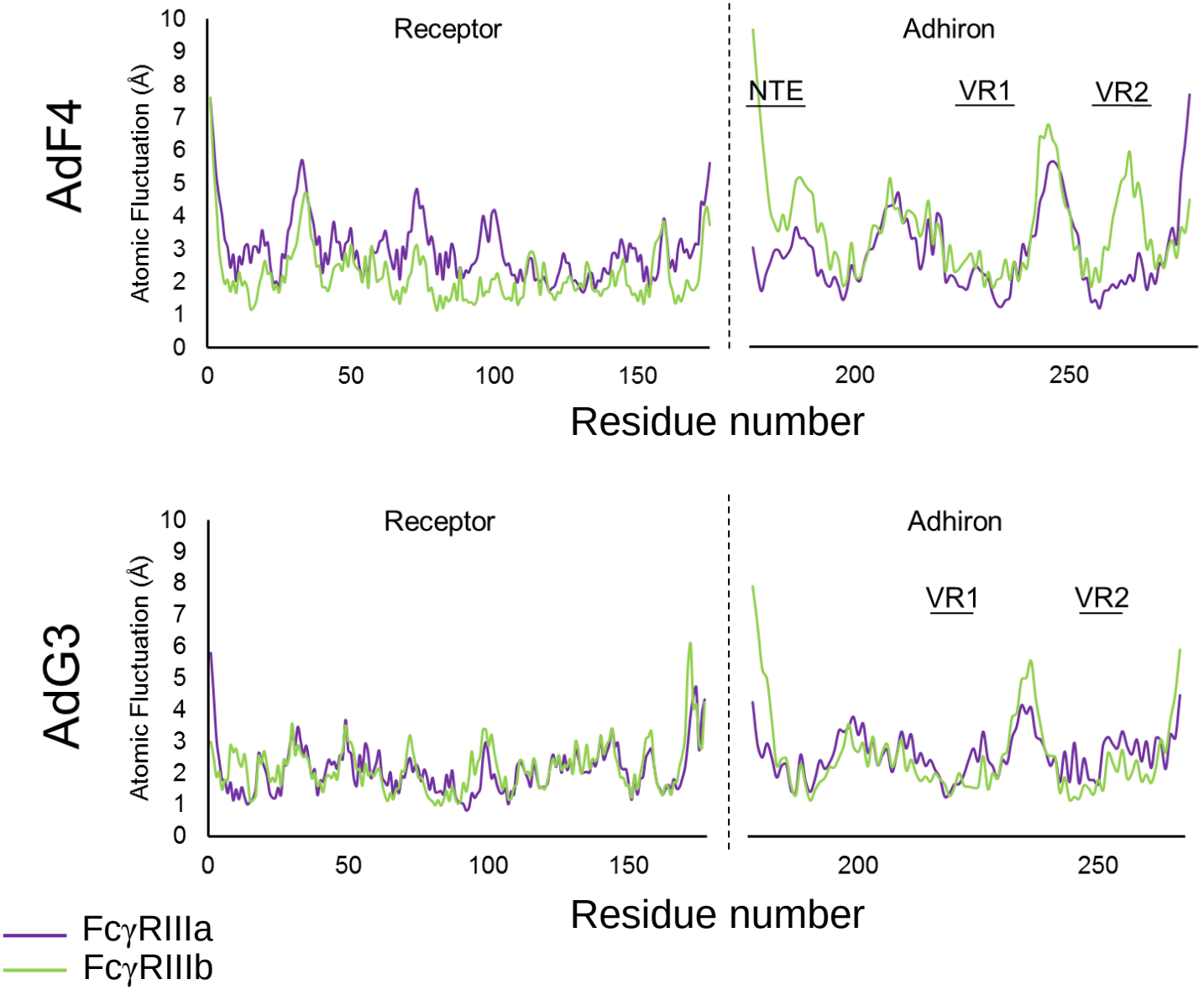
AdF4
AdG3
Receptor
Adhiron
NTE
VR1
VR2
Atomic Fluctuation (Å)
Residue number
FcγRIIIa
FcγRIIIb

Fig. S5.

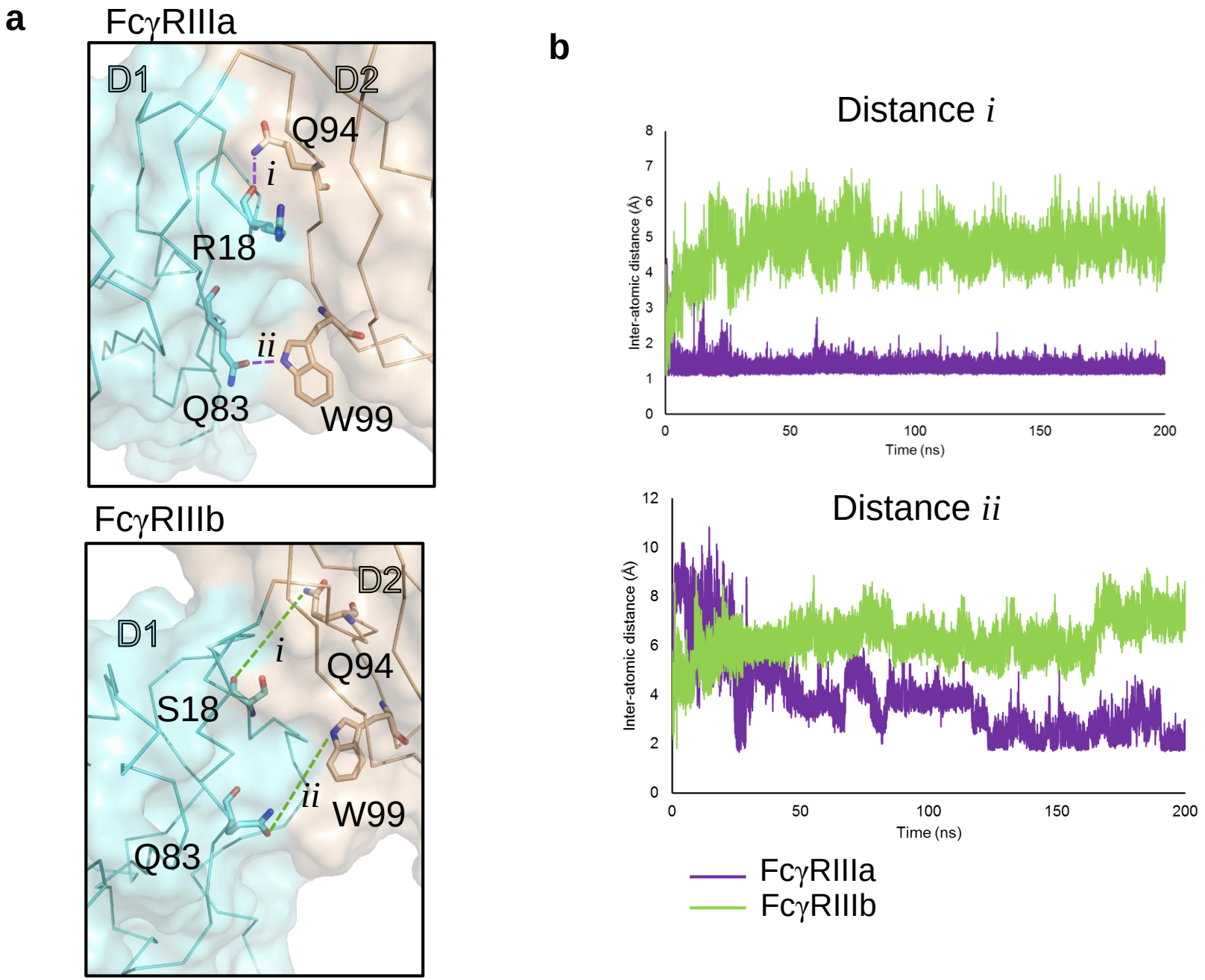
a
FcγRIIIa
D1
D2
Q94
i
R18
ii
Q83
W99
FcγRIIIb
D1
D2
i
Q94
S18
ii
W99
Q83
b
Distance i
Inter-atomic distance (Å)
Time (ns)
Distance ii
Inter-atomic distance (Å)
Time (ns)
FcγRIIIa
FcγRIIIb

Fig. S6.

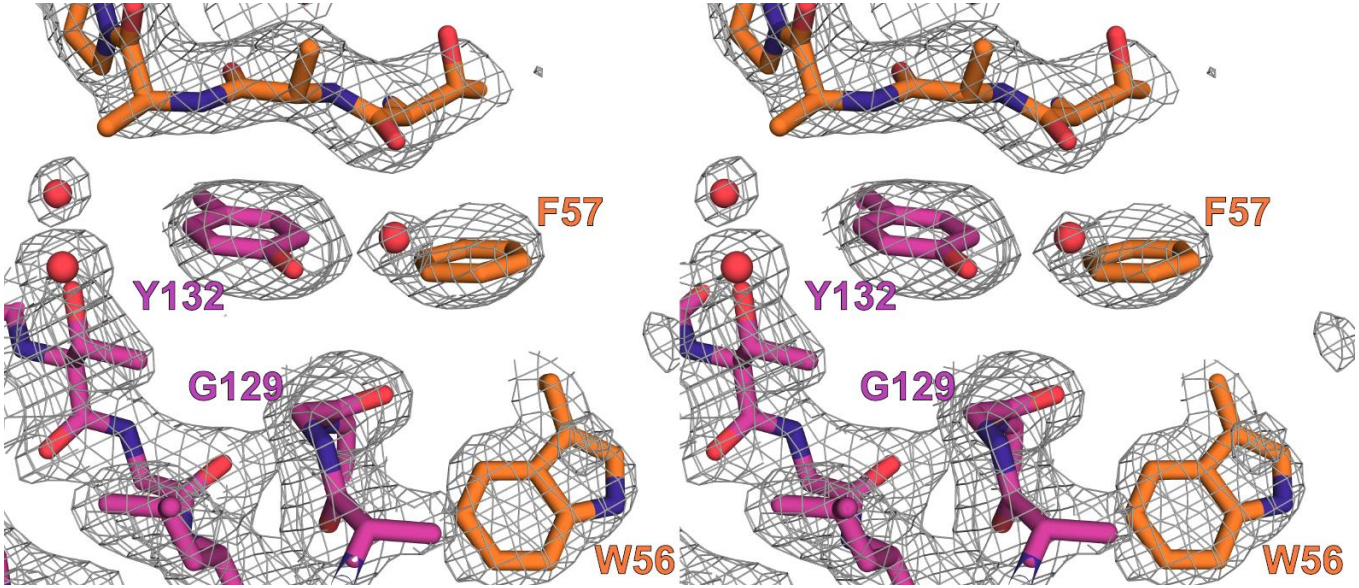

Supplementary Information

Methods

All reagents were purchased from Sigma–Aldrich (Dorset, UK) unless stated otherwise.

FcγR Cloning Strategy

FcγR ectodomains (FcγRIIIa 158F, FcγRIIa 131H) were amplified by PCR (see **Table S4** for primer sequences) and cloned into pOPINTTG (OPPF) using the InFusion system (Clontech Laboratories Inc., Mountain View, CA, USA)(32, 33).

Alternative allotypes (FcγRIIIa-158V, FcγRIIa-131R) were produced using QuikChange Lightning (Agilent Technologies, Santa Clara, CA, USA) following the Manufacturer's protocol. Constructs were tested for expression of secreted protein on a 1ml scale using transient transfection of HEK293T cells (ATCC) and analysis of the supernatant by anti-His Western blot (Roche, Indianapolis, USA), as previously described(34).

Full-length coding sequences encoding FcγRIIa (131R) and FcγRIIIb (NA2) were amplified from cDNA from peripheral blood mononuclear cells from genotyped donors. Full-length coding sequences encoding FcγRIIIa (158F) were amplified from THP-1 cells using cDNA prepared by reverse transcriptase PCR (RT-PCR) of total RNA extracted using acid phenol/ guanidinium hydrochloride and isopropanol precipitation(35) with Superscript II reverse transcriptase (Invitrogen, Paisley, Scotland) and oligo dT primers (see **Table S4** for details of primers used). These sequences were cloned into a plasmid encoding the enzymatic SNAP tag (New England Biolabs, Ipswich, MA, USA) derived from pFB HYG (a gift from Dr. J.E. Burns). The plasmids were used to transfect Phoenix A packaging cells (Nolan lab, Stanford, CA, USA) so that replication-defective virus particles were produced in the supernatant. These supernatants were filtered and used to infect HEK293 cells (in the case of FcγRIIIa–expressing cells, virus particles were used to infect cells which had already been infected with a neo resistance vector for stable expression of the common γ-chain of FcεRI gene (*FCER1G*, NM_004106.1). This double transfection was carried out to allow cell surface expression of FcγRIIIa which is dependent on the common γ-chain of FcεRI). Primer sequences for the common γ-chain of FcεRI are shown in **Table S4.** After 10 days of antibiotic selection, the cells were tested for surface expression using FITC-labelled anti-CD16 mouse monoclonal DJ130c (Dako, Glostrup, Denmark) which recognises an epitope in the first extracellular domain. This antibody was also used to show expression of FcγRIIIb. Expression of ectopically-expressed FcγRIIa was tested using mouse monoclonal AT10 (CD3204, Caltag-Medsystems, Buckingham, UK).

Protein production and purification

Proteins were secreted from HEK293T adherent cells in roller bottles. Purification was by immobilized metal affinity chromatography followed by gel filtration chromatography using a Superdex 200 column. Purified fractions were pooled and concentrated. FcγRIIIa-158F and 158V produced 1-2mg per L of culture. To produce protein for co-crystallization, the cells were grown in the presence of the glycosylation inhibitor kifunensine (Toronto Research Chemicals, ON, Canada) resulting in ectodomains with glycans of the form $Man_9GlcNAc_2$. To give protein with glycans of the form $GlcNAc_1$, the purified protein was treated with Endoglycosidase F1 overnight at 4°C and then further purified by gel filtration chromatography to remove the glycosidase and trimmed glycans from the sample. To assess the effect of FcγRIIIa glycosylation on the Adhiron interaction in SPR, the proteins were produced as above, but without Kifunensine. A portion of the glycosylated protein was treated with Endoglycosidase F1 as described.

For some experiments, FcγRIIIa ectodomains were biotinylated using EZ-link NHS-SS-biotin (Thermo Fisher Scientific, Rockford, IL), according to the manufacturer's instructions. Biotinylation was confirmed using streptavidin-conjugated to horseradish peroxidase (HRP) to detect the biotin on FcγRIIIa absorbed onto Nunc Immuno 96 Microwell™ MaxiSorp™ (Thermo Fisher Scientific, Waltham, MA, USA) plates.

In vitro selection of FcγRIIIa-specific Adhirons

a. *Phage display*

Two artificial binding protein libraries were used. The first library, referred to an as Adhiron™ library, and whose generation and screening we have previously reported(6), was constructed in-house using trimer codon-based oligonucleotides (Ella Biotech, Martinsried, Germany) and contains nine amino acid variable regions constrained within each of two loop regions. The other library (Sloning BioTechnology, Puchheim, Germany) contained a six amino acid variable N-terminal extension and the two variable loop regions. In this project aliquots of both libraries were combined for screening. In this manuscript and for the purposes of simplicity we refer to binding proteins isolated from either library as Adhirons. We used purified, endoglycosidase F1–treated and biotinylated FcγRIIIa ectodomain (158V) protein as the screening target in phage display. In brief, 5µl of the phagemid library (10^{12} colony forming units), was pre-panned three times in high binding capacity streptavidin coated wells (Thermo Fisher Scientific, Rockford, IL, USA) for a total of 1hr. The phage were

then incubated with biotinylated FcγRIIIa for 2.5hrs. Panning wells were washed 10 times and eluted with 100µl of 50 mM glycine-HCl (pH 2.2) for 10mins, neutralised with 1M Tris-HCl (pH 9.1), and further eluted with 100µl of triethylamine 100mM for 6mins and neutralised with 50µl of 1M Tris-HCl (pH 7). Eluted phage were incubated with exponentially growing ER2738 cells (OD_{600} = 0.6) for 1hr at 37°C and plated onto Lysogeny Broth (LB) agar plates. The following day phage were propagated overnight and used in a second panning round displaying FcγRIIIa on streptavidin magnetic beads. Phage/beads were incubated with mixing then washed 5 times using a KingFisher robotic platform (ThermoFisher Scientific, Rockford, IL, USA), then eluted and amplified as above. The final pan was performed using neutravidin high binding capacity plates (ThermoFisher, Scientific, Rockford, IL, USA), as described above, but the phage were eluted on a vibrating platform for 20min with 100µl 100mM dithiothreitol to reduce the disulphide bond of the EZ-link NHS-SS-biotin, prior to infection of ER2738 cells. Phage were recovered from wells containing FcγRIIIa and control wells to determine the level of amplification in target wells.

b. Binding specificity by ELISA

Phage ELISA was performed as previously described(6). Streptavidin coated plates (Thermo Fisher Scientific, Rockford, IL, USA) were blocked, labelled with 0.4 nM of biotinylated FcγRIIIa for 1hr, and 45µl of growth medium containing phage propagated from individual clones was added to wells containing biotinylated FcγRIIIa or a well containing only the biotinylated linker and incubated for 1hr. After washing 3 times in 300µl phosphate buffered saline with Tween20 (PBST), and a 1:1000 dilution of HRP-conjugated anti-phage antibody (Seramun Diagnostica GmBH, Heidesee, Germany) in 100µl PBST was added for 1hr. Wells were washed 10 times in 300µl PBST and Adhiron-mediated phage binding were visualised with 100µl 3,3′,5,5′-Tetramethylbenzidine (TMB) liquid substrate (Seramun Diagnostica GmBH, Heidesee, Germany) and absorbance measured at 560 nm. Positive binders were submitted for DNA sequence analysis (Beckman Coulter Genomics, Hope End, UK).

c. Recloning and modifications

The coding sequences of selected Adhirons were PCR amplified, restriction digested with *Nhe*I and *Pst*I and cloned into pET11a containing the Adhiron scaffold similarly digested. For biotin labelling Adhirons were cloned into a pET11a-scaffold construct encoding a C-terminal cysteine. Individual clones were sequenced to confirm the presence of the correct insert. Plasmids were transformed into BL21 (DE3) cells and cultures grown in 400ml of LB medium to an OD_{600} of 0.6 at 37°C, before addition of isopropyl β-D-1-thiogalactopyranoside to 1mM. After a further 6hr, cells were harvested, resuspended in 25ml of 1x Bugbuster (Novagen,

Nottingham, UK) with benzonase, mixed for 20min, then heated to 50°C for 20min. The cleared supernatant was mixed with 500µl Ni-NTA resin (Expedeon, San Diego CA) for 1hr, washed 3 times in 30ml wash buffer (50mM phosphate buffered saline (PBS), 500mM NaCl, 20mM imidazole, pH 7.4) and eluted in 1ml of elution buffer (50mM PBS, 500mM NaCl, 300mM imidazole, pH 7.4).

d. *Confirmation of FcγRIIIa binding*

Freshly purified Adhiron proteins were used in surface plasmon resonance (SPR) assays to confirm binding to both common FcγRIIIa allotypes (158F and V). SPR was carried out on a BIAcore T200 biosensor (GE Healthcare, Wauwotosa WI, USA). Soluble FcγRIIIa ectodomains of the 158V allotype were immobilised (100RU) in 10mM acetate pH5.0 on a CM5 sensor chip (GE Healthcare) using amine coupling, as directed by the manufacturer. Adhirons were used as analytes in single cycle kinetics with 2min injections of increasing concentrations from 123nM through to 10µM at a flow rate of 30µl/min in HBS-EP+ running buffer. The FcγRIIIa surface was regenerated between cycles using a 60s injection of 10mM glycine pH2.0 at 30µl/min.

A blank amine coupled flow cell was used as reference and zero concentration controls were used in double-referencing. All analysis was carried out using the BIAcore T200 Evaluation Software v1.0. Langmuir 1:1 kinetic models were fitted to reference-subtracted sensorgrams and steady state affinity models were fitted.

For isothermal titration calorimetry (ITC), protein samples were dialysed against PBS overnight at 4°C and this buffer was used for control titrations. ITC was performed using an iTC200 instrument (Microcal, Malvern Instruments) at 25°C. An initial injection of 0.5µl over 1 second was followed by 19 injections of 2µl over 4 seconds each, with 2 minute spacing, while stirring at 750rpm and with a reference power of 5µCal/sec. The sample cell contained 10µM FcγRIIIa-158V and Adhiron was injected at a concentration of 100µM. Results were analysed using Origin software after subtraction of a control titration of Adhiron into buffer.

Cell-based IgG binding assays

Constructs encoding FcγRIIa (27Q 131H), FcγRIIIa (158F and V) and FcγRIIIb-NA2 were stably transfected into HEK293 cells and used to investigate FcγRIIIa-specific inhibition of IgG1 HAG binding. Cells were harvested with trypsin and EDTA then resuspended at 250 cells/µl in Dulbecco's Modified Eagle's medium (Invitrogen, Paisley, UK) containing 10% fetal calf serum (FCS). Each selected Adhiron was added at 50µg/ml incubated at room temperature for 1hr. The cells were cooled on ice and incubated with 100µg/ml heat-

aggregated gamma globulin (HAG) (The Binding Site, Birmingham, UK) for a further 2 hours. The cells were incubated on ice for 1hr with 100x diluted goat anti-human κ light chain $F(ab')_2$ fragments labelled with phytoerythrin (PE) (AbD Serotec, BioRad, Hercules, CA, USA). Cells were washed in ice-cold FACS buffer (PBS with 2%FCS and 2mM EDTA) then fixed in 2% formaldehyde to prevent loss or phagocytosis of complexes. Binding of HAG to the FcγR-expressing cells was assessed using a Guava EasyCyte Flow Cytometer (Millipore, Watford, UK) using empty vector–transfected cells as controls.

The median fluorescence Intensity (MFI) was determined for each tube and averages of triplicate values were determined for each cell line. Statistical significance was calculated by using two-tailed Student's *t*-tests for inhibition of HAG binding and an assumption of unequal variance.

Blockade of effector functions in the THP-1 macrophage cell line

a. Characterization of the FcγR expression on THP-1 cells under different culture conditions.

In order to select suitable monoclonal antibodies for these studies we undertook some genetic and transcriptional analysis of the THP-1 cell line. The extracellular domains of the CD32 receptors (FcγRIIa, FcγRIIb and FcγRIIc) are almost identical and consequently not all CD32 mAbs are able to fully distinguish between the FcγRII subtypes. CD32-IV3 (Stem cell Technologies, Marseille, France) has been reported to recognise only FcγRIIa (36, 37). Whereas, CD32 3D3 (BD Pharmingen, Oxford, UK) recognises FcγRIIa-131R, FcγRIIb and FcγRIIc. The THP-1 cell line was therefore genotyped for *FCGR2A*-131H/R by direct sequencing of genomic DNA, using published assays (38). The *FCGR2C* STP/ORF variant and transcription of specific FcγRIIb/c isoforms were determined as described in (39).

Human monocytic THP-1 cells (European Collection of Cell Cultures) were grown in RPMI 1640 containing 10% FCS, 2mM L-glutamine at 37°C in 5% CO_2. The level of FcγR cell surface expression was initially determined in resting and PMA-differentiated THP-1 cells. Briefly, THP-1 cells were seeded at a density of 2 $x10^5$ cells/ml and incubated with media alone or 50ng/ml PMA for 18hr at 37°C. The medium containing PMA was removed and the cells rested for 48hr in the presence of medium alone.

The level of expression of cell surface markers (FcγRIII: CD16-3G8, Caltag-Medsystems, Buckingham, UK, CD32-IV.3, Stem cell Technologies, Marseille, France) and CD32-3D3, BD Pharmingen, Oxford, UK, CD64-10.1, Beckman Coulter Immunotech, Marseille, France) and the percentage of cells positive for these markers were evaluated in differentiated THP-1 cells incubated for an additional 24hr in the presence of medium alone or following

stimulation with 250ng/ml lipopolysaccharide (LPS). Cells harvested using trypsin and EDTA were washed in PBS-bovine specific albumin (BSA), stained with directly conjugated antibodies (diluted 250x, 30min, 4°C, in dark), washed with PBS-BSA, resuspended in PBS-BSA and analysed by flow cytometry (Becton Dickinson LSRII, Oxford, UK).

a. TNF production

TNF production was assessed in differentiated THP-1 cells (2 x 10^5 cells in 500µl) that were incubated for 1hr at 37°C in medium alone (negative control), or with 250ng/ml LPS (positive control) or with 100µg/ml HAG prior to addition of 10µg/ml brefeldin A (intracellular protein transport inhibitor) and further incubation for 3hr (37°C, 5% CO_2). Blocking antibodies were obtained from Ancell Corporation (Bayport MN). The antibody clones were 3G8 for CD16 (a known blocking Ab), 7.3 for CD32 and 10.1 for CD64. Cells were washed in PBS- 2%BSA, fixed in 2% paraformaldehyde for 30min, washed again and then permeabilized using 0.3% saponin in PBS-BSA (15min, room temp.). Anti-TNF-phycoerythrin (PE) or IgG1-PE (Serotec, Oxford, UK) diluted 1: 500 in PBS-BSA + 0.1% saponin were added for 30min (room temp. in dark), washed and resuspended in PBS-BSA for immediate analysis by flow cytometry (Becton Dickinson LSRII, Oxford, UK).

b. *Phagocytosis of IgG-opsonised* E. coli

Phagocytosis was assessed by incubation of differentiated THP-1 cells (2 x 10^5 cells/ml) with either 10 µg/ml *E. coli* (Invitrogen, Paisley, UK) alone or *E. coli* pre-opsonised with 5% human AB serum (complement inactivated: 56°C, 30min), followed by washing (1600 x g, 15min) to remove excess serum) for 1hr at 37°C, or in cells pre-cooled to 4°C (negative control). Cells were washed in PBS-BSA, stained with 0.4% trypan blue to quench extracellular fluorescence, washed three times with PBS-BSA and resuspended in PBS-BSA and analysed by cytometry (Becton Dickinson, LSRII, Oxford, UK).

Crystallisation and Structure Solution

Endoglycosidase F1-treated FcγRIIIa crystals 20-30 µm in size were grown in 200nl drops (100nl FcγRIIIa ectodomain + 100nl precipitant) in 96-well plates using non-contact dispensing robotics (Microsys Cartesian, Romania). Crystallization trials used the method of Walter *et al.*(40) at 8.9 mg/ml for 158F and at 11.4 mg/ml for 158V. Co-crystallization of FcγRIIIa with Adhirons was performed by mixing the proteins in a 1:1 molar ratio and incubating at room temperature for 30mins before setting up crystallization trials. Conditions are shown in **Table S3**.

Crystals were detected in a number of conditions with data being collected from condition 41 or 43 of the Hampton PEG / Ion screen (20% (w/v) Polyethylene Glycol 3350, 0.200 M Potassium di-Hydrogen Phosphate and 20% (w/v) Polyethylene Glycol 3350, 0.200 M Ammonium Phosphate Monobasic) or optimizations around these conditions(40).

For diffraction data collection, crystals were loop mounted and cryo-cooled in liquid nitrogen. Data were collected at Beamline I24, Diamond Light Source, with the X-ray beam defocused to 20×20 μm^2 from multiple positions on each crystal. All diffraction data were integrated using XDS(41) and scaled using AIMLESS(42). Phases were obtained via molecular replacement using PHASER(43). A subsection of a complex of an Adhiron bound to a soluble protein (manuscript in preparation) was used as a search model. Refinement was carried out using PHENIX(44). Ligands and sugar modifications were built manually into *Fo-Fc* maps using COOT(45). In the case for AdG3 additional noncrystallographic symmetry torsion restraints were applied during refinement. The quality of the protein structure was assessed using MOLPROBITY. Data collection and refinement statistics are given in Table 1.

The residues involved in Adhiron binding to FcγRIIIa were identified based on the Protein Interaction Calculator(46) and visual inspection.

Molecular dynamics simulations.

Molecular dynamics (MD) simulations were prepared with the AmberTools 14 suite of programs and performed with AMBER14 (47), ff14SB47 (48) and GLYCAM_06j-1 (49). Simulations used 128 processors of the MARC1 supercomputer available at Leeds. To simulate Adhiron-FcγR interactions in water, models were first generated of each Adhiron in complex with either FcγRIIIa (-158F allotype for AdG3 and -158V allotype for AdF4) or FcγRIIIb-NA2. The FcγRIIIb-containing complex was generated by mutation of the FcγRIIIa-Adhiron crystal structures to resemble the FcγRIIIb-NA2 through the use of TRITON/MODELLER (50).

After mutagenesis, the xleap program of AmberTools 14 was used to add hydrogen atoms, form disulphide bridges and add β1,4 linked D-N-acetyl glucosamine (GlcNAc) residues at glycosylation sites in FcγRIIIa/FcγRIIIb. Complexes were then placed in a TIP3P water box with a 10.0-Å cut-off, and the system was neutralized with Na+ ions. The system was equilibrated through an initial energy minimization, which was followed by 80ps of restrained molecular dynamics during which the system was heated to 300K with gradual releasing of restraints. An unrestrained MD simulation of 200ns was then performed. For each complex, simulations were repeated in triplicate.

Calculations of the Root Mean Square Deviation (RMSD) showed that all simulations remained stable, and that 200ns was sufficient for the RMSD to converge to a stable value, which indicates that no significant global conformational changes are taking place over MD timescales.

Desolvated trajectories were analysed with the cpptraj module of AMBER14, which was used to calculate inter- and intra-molecular H-bonds, per residue atomic fluctuations and inter-atomic distances. H-bonds with a cutoff of 3.2- Å and 160°, which were present for more than 5% of the total trajectory, were recorded. VMD was used to render videos of the simulations and PyMOL was used to generate representative figures (51, 52).

Table S1. List of specific interactions at Adhiron / protein interface seen in crystal structure 5ML9.

	FcγRIIIa		distance in Å	water	distance in Å	Adhiron F4		
125	GLN	[Oε1]	2.7	--	--	55	HIS	[Nε2]
130	ARG	[O]	2.9	--	--	57	PHE	[N]
130	ARG	[Nε]	2.5	--	--	55	HIS	[O]
130	ARG	[Nε2]	3.1	11	2.9	54	GLU	[O]
131	LYS	[Nω2]	2.7	--	--	58	PRO	[O]
131	LYS	[Nω2]	2.7	--	--	60	THR	[Oγ1]
132	TYR	[N]	2.8	--	--	85	ASN	[Nδ2]
132	TYR	[N]	2.8	1	2.6	85	ASN	[N]
134	HIS	[N]	2.4	--	--	19	GLU	[Oε2]
134	HIS	[Nε2]	2.7	--	--	22	GLU	[Oε2]
135	HIS	[N]	3.1	--	--	19	GLU	[Oε2]
135	HIS	[Nε2]	2.5	--	--	22	GLU	[Oε2]
136	ASN	[O]	2.5	37	2.6	19	GLU	[N]
137	SER	[Oγ]	3.1	--	--	16	ASN	[Nδ2]
137	SER	[Oγ]	2.8	50	2.9	16	ASN	[Nδ2]
138	ASP	[N]	2.6	--	--	16	ASN	[Oδ1]
--	--	--	--	50	2.9	62	THR	[Oγ1]
--	--	--	--	50	2.7	49	GLU	[Oε2]

Table S2: Average B factor per chain of AdG3.

Chain	Average B
A	66.1
B	104.2
C	73.6
D	76.5
water	62.8
all	80.1

Table S3. List of specific interactions at Adhiron / protein interface seen in crystal structure 5MN2.

FcγRIIIa			distance in Å	water	distance in Å	Adhiron G3		
17	TYR	[OH]	2.8	1	2.8	85	HIS	[O]
83	GLN	[Nε2]	2.7	--	--	83	GLN	[O]
83	GLN	[Oε1]	2.6	2	2.9	83	GLN	[N]
85	GLU	[Oε2]	2.8	--	--	85	HIS	[N]
85	GLU	[Oε2]	2.6	1	--	--	--	--
86	VAL	[N]	3.2	37	3	85	HIS	[Nε2]
99	VAL	[N]	3.2	--	--	51	GLY	[O]
167	THR	[Oγ1]	3.4	--	--	86	ASN	[Nδ2]
169	ASN	[N]	3.1	--	--	83	GLN	[Oε1]
169	ASN	[O]	2.9	--	--	83	GLN	[Nε2]
--	--	--	--	2	2.9	83	GLN	[O]
--	--	--	--	2	2.8	52	PHE	[O]
--	--	--	--	2	3.0	98	TRP	[Nε]
--	--	--	--	37	3	86	VAL	[O]

		FcγRIIIa-AdG3			FcγRIIIb NA2-AdG3		
Donor residue	**Acceptor residue**	**Occupancy (%)**	**Avg Dist (Å)**	**Avg Angle (°)**	**Fraction of simulation**	**Average distance**	**Average angle**
Inter-molecular H-bonds							
FcγR-Trp98 (N)	AdG3-Gly52 (O)	26.14	2.91	159.11	15.92	2.85	151.78
FcγR-Val99 (N)	AdG3-Gly52 (O)	44.22	2.89	161.24			
FcγR-Arg18 (NH1/NH2)	AdG3-Asn86 (OD1)	39.30	2.84	152.25			
Intra-molecular H-bonds							
Gln94 (NE2)	Arg/Ser18 (O)	69.53	2.85	162.62	26.38	2.76	157.72
Glu21 (H)	Arg/Ser18 (O)				37.44	2.88	154.16
Leu20 (H)	Arg/Ser18 (O)				57.48	2.85	159.65
Arg/Ser18 (H)	Ala95 (O)	32.87	2.87	151.96			
Arg18 (NH1/NH2)	Glu166 (OE2)	35.71	2.81	151.90			
Arg18 (NH1/NH2)	Glu166 (OE1)	19.15	2.81	151.57			
Trp98 (HE2)	Gln83 (OE1)	38.31	2.84	156.71			

Table S3. Selected H bond distances in the key interactions between FcγRIIIa/b and AdG3 in molecular dynamics simulations.

Table S4: Protein/Adhiron crystallization conditions.

Protein	Adhiron	Screen	Conditions
FcγRIIIa 158F	AdG3	JCGS+ (D12)	20.0% v/v Glycerol 16.0% w/v Polyethylene glycol 8000 0.04 M Potassium di-Hydrogen Phosphate
FcγRIIIa 158V	AdF4	JCSG+ (E2)	2.0 M Ammonium Sulphate 0.1 M Sodium Cacodylate pH=6.50 0.2 M Sodium Chloride

Table S6: List of sugar-modified residues.

FcγRIIIa-AdG3	**FcγRIIIa-AdF4**
A Asn38	A Asn45
A Asn45	A Asn74
A Asn74	A Asn169
A Asn162	
A Asn169	
B Asn45	
B Asn74	

Table S7: Cloning primer sequences.

Primer name	Vector / Fragment	Size (bp)	Sequence (5'-3')
FCGR2A ectoF	pOPINTTG 2Aectodomain	551	GCGTAGCTGAAACCGGCGCTCCCCCAAAGGCTGTGC
FCGR2A ectoR			GTGATGGTGATGTTTGCTGGGCACTTGGACAGTGATGG
FCGR2A SDMF	pOPINTTG 2Aectodomain 131R	551	TCCCAGAAATTCTCCCGTTTGGATCCCACCTTC
FCGR2A SDMR			GAAGGTGGGATCCAAACGGGATTTCTGGGA
FCGR3A ectoF	pOPINTTG 3A ectodomain	551	GCGTAGCTGAAACCGGCGAAGATCTCCCAAAGGCTGTGGTG
FCGR3A ectoR			GTGATGGTGATGTTTACCTTGAGTGATGGTGATGTTCACAG
pFBHYGFCGR2AF	pFBHYGSNAP 2A full length	986	AATTGTCGACGAATTCATGACTATGGAGACCCAAATGTC
FCGR2A SNAPR			CTTTGTCCATGGATCCGTTATTACTGTTGACATGGTC
pFBHYGFCGR3AF	pFBHYGSNAP 3A full length	905	AATTGTCGACGAATTCATGGGTGGAGGGGCTGGGGAA
FCGR3A SNAPR			CTTTGTCCATGGATCCTTTGTCAGGGTCTTTTCTCCA
FCGR3ASDMf	pFBHYGSNAP 3A full length 158V	905	CTTCTGCAGGGGGCTCTTGTTGGGAGTAAAAATGT
FCGR3ASDMr			ACATTTTTACTCCCAACAAGCCCCCTGCAGAAG
pFBHYGFCGR3AF	pFBHYG 3B full length	842	AATTGTCGACGAATTCATGGGTGGAGGGGCTGGGGAA

FCGR3B R			GCCGCTCGAGGATCCTCAAATGTTTGTCTTCACAGAG

Supplementary Figure Legends

Figure S1. FcγRIIIa interactions with AdF4 and AdG3 (123nM-10μM) by surface plasmon resonance. (**a**) Amine coupled receptors. Single cycle kineticsA 1:1 binding model (superimposed red line) provided kinetic measurements of association (k_a) and dissociation (k_d) and equilibrium dissociation constant (K_D) as indicated. Interaction kinetics exceeded the measurement capabilities of the instrument at higher Adhiron concentrations. (**b**) Orientated C-terminal Avitag-immobilised receptors. Steady-state affinity measurements from SPR for each Adhiron interaction with immobilised fully glycosylated and Endo F1-treated FcγRIIIa.

Figure S2. Overlapping binding sites on FcγRIIIa for IgG Fc and AdF4. FcγRIIIa-IgG Fc from 3SGJ (yellow) and -AdF4 from 5ML9 (red) interfaces overlap by ~50% (orange) illustrating the steric nature of the IgG inhibition. Interface surface areas were calculated using PISA (EMBL-EBI).

Figure S3. Per-residue Root Mean Square Deviation (RMSD) analysis of FcγRIIIa/b-AdF4 and -AdG3 molecular dynamics trajectories. RMSD values were averaged over three repeats and show that all simulations remained stable during the timescale of the simulations, and that 200ns was sufficient for the RMSD to converge to a stable value.

Figure S4. Atomic fluctuation by residue of FcγRIIIa/b-AdF4 and –AdG3 molecular dynamics trajectories. Higher values represent greater fluctuation. All values were averaged over three repeats. Purple plots represent FcγRIIIa-containing simulations and green plots represent FcγRIIIb-containing simulations.

Figure S5. Molecular dynamics simulations suggest proposed mechanism of AdG3-mediated FcγRIIIa inter-domain angle restriction. (a) View of D1-D2 interdomain hinge in FcγRIIIa and FcγRIIIb after 200ns of molecular dynamics simulation, D1 depicted in aqua marine, D2 depicted in wheat. **(b)** Measurements i and ii describe interatomic distances over the course of the 200ns AdG3 simulations for both FcγRIIIa (purple lines) and FcγRIIIb (green lines) averaged over three repeats. Formation of the γaArg18-γaGln94 H-bond early in the simulations leads to formation of an additional interdomain H-bond between γaGln83 and γaTrp99. In FcγRIIIb the lack of i formation leads to greater flexibility between D1 and D2 preventing the formation of ii.

Figure S6. Stereo image of AdF4-FcγRIIIa ectodomain model fitted to electron density map contoured at 2.0 sigma. FcγRIIIa in purple stick and AdF4 in orange stick representation.

1. Berrow NS, Alderton D, & Owens RJ (2009) The Precise Engineering of Expression Vectors Using High-Throughput In-Fusiontrade mark PCR Cloning. *Methods Mol Biol* 498:75-90.
2. Bird LE (2011) High throughput construction and small scale expression screening of multi-tag vectors in Escherichia coli. *Methods* 55:29-37.
3. Nettleship JE, Rahman-Huq N, & Owens RJ (2009) The production of glycoproteins by transient expression in mammalian cells. *Methods Mol Biol* 498:245-263.
4. Chomczynski P & Sacchi N (1987) Single-step method of RNA isolation by acid guanidinium thiocyanate -phenol-chloroform extraction. *Analytical Biochemistry* 162(1):156-159.
5. Warmerdam PAM*, et al.* (1993) Interaction of a human FcγRIIb1 (CD32) isoform with murine and human IgG subclasses. *Int Immunol* 5:239-247.
6. Daeron M*, et al.* (1995) The same tyrosine-based inhibition motif, in the intracytoplasmic domain of Fc gamma RIIB, regulates negatively BCR-, TCR-, and FcR-dependent cell activation. *Immunity* 3(5):635-646.
7. Morgan AW*, et al.* (2006) Analysis of Fcγ Receptor haplotypes in rheumatoid arthritis. *FCGR3A* remains a major susceptibility gene at this locus with an additional contribution from *FCGR3B*. *Arthritis Research & Therapy* 8:R5.
8. Metes D*, et al.* (1998) Expression of functional CD32 molecules on human NK cells is determined by an allelic polymorphism of the FcγRIIC gene. *Blood* 91(7):2369-2380.
9. Walter TS*, et al.* (2005) A procedure for setting up high-throughput nanolitre crystallization experiments. Crystallization workflow for initial screening, automated storage, imaging and optimization. *Acta Crystallogr D Biol Crystallogr.* 61:651-657.
10. Kabsch W (2010) XDS. *Acta Crystallographica Section D* 66(2):125-132.
11. Evans PR & Murshudov GN (2013) How good are my data and what is the resolution? *Acta Crystallographica Section D* 69(7):1204-1214.
12. McCoy AJ*, et al.* (2007) Phaser crystallographic software. *Journal of Applied Crystallography* 40(Pt 4):658-674.
13. Afonine PV*, et al.* (2012) Towards automated crystallographic structure refinement with phenix.refine. *Acta Crystallographica Section D* 68(4):352-367.
14. Emsley P, Lohkamp B, Scott WG, & Cowtan K (2010) Features and development of Coot. *Acta Crystallographica Section D* 66(4):486-501.
15. Tina KG, Bhadra R, & Srinivasan N (2007) PIC: Protein Interactions Calculator. *Nucleic Acids Res* 35:W473-W476.
16. Case DA*, et al.* (2014) *{Amber 14}*.
17. Maier JA*, et al.* (2015) ff14SB: Improving the Accuracy of Protein Side Chain and Backbone Parameters from ff99SB. *Journal of Chemical Theory and Computation* 11(8):3696-3713.
18. Prokop M, Adam J, Kříž Z, Wimmerová M, & Koča J (2008) TRITON: a graphical tool for ligand-binding protein engineering. *Bioinformatics* 24(17):1955-1956.
19. Onufriev A, Bashford D, & Case DA (2000) Modification of the Generalized Born Model Suitable for Macromolecules. *The Journal of Physical Chemistry B* 104(15):3712-3720.
20. Humphrey W, Dalke A, & Schulten K (1996) VMD: visual molecular dynamics. *J Mol Graph* 14(1):33-38, 27-38.

21. Anonymous (*The PyMOL Molecular Graphics System, Version 1.2r3pre* (Schrödinger, LLC).